



CERN-EP-2017-135
LHCb-PAPER-2017-015
10th July 2017

Study of prompt D^0 meson production in $p\text{Pb}$ collisions at $\sqrt{s_{\text{NN}}} = 5 \text{ TeV}$

The LHCb collaboration[†]

Abstract

Production of prompt D^0 mesons is studied in proton-lead and lead-proton collisions recorded at the LHCb detector at the LHC. The data sample corresponds to an integrated luminosity of $1.58 \pm 0.02 \text{ nb}^{-1}$ recorded at a nucleon-nucleon centre-of-mass energy of $\sqrt{s_{\text{NN}}} = 5 \text{ TeV}$. Measurements of the differential cross-section, the forward-backward production ratio and the nuclear modification factor are reported using D^0 candidates with transverse momenta less than $10 \text{ GeV}/c$ and rapidities in the ranges $1.5 < y^* < 4.0$ and $-5.0 < y^* < -2.5$ in the nucleon-nucleon centre-of-mass system.

Submitted to JHEP

© CERN on behalf of the LHCb collaboration, licence CC-BY-4.0.

[†]Authors are listed at the end of this paper.

1 Introduction

Charm hadrons produced in hadronic and nuclear collisions are excellent probes to study nuclear matter in extreme conditions. The differential cross-sections of c -quark production in pp or $p\bar{p}$ collisions have been calculated based on perturbative quantum chromodynamics (QCD) and collinear or k_T factorisation [1–6]. These phenomenological models [7] are also able to predict the differential cross-section of c -quark production including most of the commonly assumed “cold nuclear matter” (CNM) effects in nuclear collisions, where CNM effects related to the parton flux differences and other effects come into play. Since heavy quarks are produced at a time scale of approximately 0.1 fm/ c after the collision, they are ideal to examine hot nuclear matter, the so-called “quark-gluon plasma” (QGP), by studying how they traverse this medium and interact with it right after their formation. These studies require a thorough understanding of the CNM effects, which can be investigated in systems where the formation of QGP is not expected. In addition, a precise quantification of CNM effects would significantly improve the understanding of charmonium and open-charm production by confirming or discarding the possibility that the suppression pattern in the production of quarkonium states, like J/ψ , at the SPS, RHIC and LHC is due to QGP formation [7].

The study of CNM effects is best performed in collisions of protons with heavy nuclei like lead, where the most studied CNM effects, such as gluon saturation [8, 9] and in-medium energy loss [10] in initial- and final-state radiation [11, 12], are more evident. Phenomenologically, collinear parton distributions are often used to describe the nuclear modification of the parton flux in the nucleus. The modification with respect to the free nucleon depends on the parton fractional longitudinal momentum, x , and the atomic mass number of the nucleus A [13, 14]. In the low- x region, down to $x \approx 10^{-5} - 10^{-6}$, which is accessible at LHC energies, stronger onset of gluon saturation [15–18] is expected to play a major role. Its effect can be quantified by studying production of D^0 mesons at low transverse momentum p_T [19], ideally down to zero p_T . The in-medium energy loss occurs when the partons lose energy in the cold medium through both initial- and final-state radiation.

CNM effects have been investigated in detail at the RHIC collider in pp and dAu collisions [7, 20] at a nucleon-nucleon centre-of-mass energy of $\sqrt{s_{NN}} = 200$ GeV. Most recently, CNM effects were measured in pPb collisions at the LHC for quarkonium and heavy flavour production [21–36]. The ALICE experiment [28] studied D meson production in pPb collisions at $\sqrt{s_{NN}} = 5$ TeV in the region $0.96 < y^* < 0.04$ for $p_T > 2$ GeV/ c , where y^* is the rapidity of the D meson defined in the centre-of-mass system of the colliding nucleons. Their results suggest that the suppression observed in PbPb collisions is due to hot nuclear matter effects, *i.e.* QGP formation. Results on leptons from semileptonic heavy-flavour decays at various rapidities are also available [37–39].

In this paper the measurement of the cross-section and of the nuclear modification factors of “prompt” D^0 mesons, *i.e.* those directly produced in proton-lead collisions and not coming from decays of b -hadrons, is presented. The measurement is performed at $\sqrt{s_{NN}} = 5$ TeV with the LHCb [40] detector at the LHC. Depending on the direction of the proton and ^{208}Pb beams and due to the different energies per nucleon in the two beams, the LHCb detector covers two different acceptance regions in the nucleon-nucleon rest frame,

- $1.5 < y^* < 4.0$, denoted as “forward” beam configuration,
- $-5.0 < y^* < -2.5$, denoted as “backward” beam configuration,

where the rapidity y^* is defined with respect to the direction of the proton beam, The measurement is performed in the range of D^0 transverse momentum $p_T < 10 \text{ GeV}/c$, in both backward and forward collisions.

2 Detector and data samples

The LHCb detector [40, 41] is a single-arm forward spectrometer covering the pseudorapidity range $2 < \eta < 5$, designed for the study of particles containing b or c quarks. The detector includes a high-precision tracking system consisting of a silicon-strip vertex detector surrounding the pp interaction region (VELO), a large-area silicon-strip detector (TT) located upstream of a dipole magnet with a bending power of about 4 Tm, and three stations of silicon-strip detectors and straw drift tubes (OT) placed downstream of the magnet. The tracking system provides a measurement of momentum, p , of charged particles with a relative uncertainty that varies from 0.5% at low momentum to 1.0% at 200 GeV/ c . The minimum distance of a track to a primary vertex (PV), the impact parameter, is measured with a resolution of $(15 + 29/p_T) \mu\text{m}$, where p_T is the component of the momentum transverse to the beam, in GeV/ c . Different types of charged hadrons are distinguished using information from two ring-imaging Cherenkov detectors. Photons, electrons and hadrons are identified by a calorimeter system consisting of scintillating-pad and preshower detectors, an electromagnetic calorimeter and a hadronic calorimeter. Muons are identified by a system composed of alternating layers of iron and multiwire proportional chambers. The online event selection is performed by a trigger [42], which consists of a hardware stage, based on information from the calorimeter and muon systems, followed by a software stage, which applies a full event reconstruction.

The data sample used in this analysis consists of $p\text{Pb}$ collisions collected in early 2013, corresponding to integrated luminosities of $(1.06 \pm 0.02) \text{ nb}^{-1}$ and $(0.52 \pm 0.01) \text{ nb}^{-1}$ for the forward and backward colliding beam configurations, respectively. The luminosity has been determined using the same method as in the LHCb measurement of J/ψ production in $p\text{Pb}$ collisions [43], with a precision of about 2%. The instantaneous luminosity during the period of data taking was around $5 \times 10^{27} \text{ cm}^{-2} \text{ s}^{-1}$, which led to an event rate that was three orders of magnitude lower than in nominal LHCb pp operation. Therefore, the hardware trigger simply rejected empty events, while the next level software trigger accepted all events with at least one track in the VELO.

For the analyses presented below, simulated samples of pp collisions at 8 TeV are used to determine geometrical acceptance and reconstruction efficiencies. Effects due to the different track multiplicity distributions in the pp and $p\text{Pb}$ collision data and the effects of the asymmetric beam energies in $p\text{Pb}$ collisions are taken into account as described later. In the simulation, pp collisions are generated using PYTHIA [44] with a specific LHCb configuration [45]. Decays of hadronic particles are described by EVTGEN [46], in which final-state radiation is generated using PHOTOS [47]. The interaction of the generated particles with the detector, and its response, are implemented using the GEANT4 toolkit [48, 49].

3 Cross-section determination

The double-differential cross-section for prompt D^0 production in a given (p_T, y^*) kinematic bin is defined as

$$\frac{d^2\sigma}{dp_T dy^*} = \frac{N(D^0 \rightarrow K^\mp \pi^\pm)}{\mathcal{L} \times \varepsilon_{\text{tot}} \times \mathcal{B}(D^0 \rightarrow K^\mp \pi^\pm) \times \Delta p_T \times \Delta y^*}, \quad (1)$$

where $N(D^0 \rightarrow K^\mp \pi^\pm)$ is the number of prompt D^0 signal candidates reconstructed through the $D^0 \rightarrow K^\mp \pi^\pm$ decay channels¹, ε_{tot} is the total D^0 detection efficiency, \mathcal{L} is the integrated luminosity, $\mathcal{B}(D^0 \rightarrow K^\mp \pi^\pm) = (3.94 \pm 0.04)\%$ is the sum of the branching fractions of the decays $D^0 \rightarrow K^- \pi^+$ and $D^0 \rightarrow K^+ \pi^-$ [50], $\Delta p_T = 1 \text{ GeV}/c$ is the bin width of the D^0 transverse momentum, and $\Delta y^* = 0.5$ is the bin width of the D^0 rapidity. The rapidity y^* is defined in the nucleon-nucleon centre-of-mass frame, where the positive direction is that of the proton beam. The measurement is performed in the D^0 kinematic region defined by $p_T < 10 \text{ GeV}/c$ and rapidities $1.5 < y^* < 4.0$ for the forward sample and $-5.0 < y^* < -2.5$ for the backward sample.

The total cross-section over a specific kinematic range is determined by integration of the double-differential cross-section. The nuclear modification factor, $R_{p\text{Pb}}$, is the ratio of the D^0 production cross-section in forward or backward collisions to that in pp at the same nucleon-nucleon centre-of-mass energy $\sqrt{s_{\text{NN}}}$

$$R_{p\text{Pb}}(p_T, y^*) \equiv \frac{1}{A} \frac{d^2\sigma_{p\text{Pb}}(p_T, y^*)/dp_T dy^*}{d^2\sigma_{pp}(p_T, y^*)/dp_T dy^*}, \quad (2)$$

where $A=208$ is the atomic mass number of the lead nucleus. The forward-backward production ratio, R_{FB} , is defined as

$$R_{\text{FB}}(p_T, y^*) \equiv \frac{d^2\sigma_{p\text{Pb}}(p_T, +|y^*|)/dp_T dy^*}{d^2\sigma_{\text{Pb}p}(p_T, -|y^*|)/dp_T dy^*}, \quad (3)$$

where $\sigma_{p\text{Pb}}$ and $\sigma_{\text{Pb}p}$ indicate the cross-sections in the forward and backward configurations respectively, measured in a common rapidity range. The D^0 candidates are selected according to the same requirements as used in the D^0 production cross-section measurements in pp collisions at $\sqrt{s} = 7 \text{ TeV}$ [51] and $\sqrt{s} = 13 \text{ TeV}$ [52]. The kaon and pion tracks from the D^0 candidate and the vertex they form are both required to be of good quality. The requirements set on particle identification (PID) criteria are tighter than in pp collisions to increase the signal-over-background ratio given the high detector occupancy observed in $p\text{Pb}$ collisions.

The signal yield is determined from an extended unbinned maximum likelihood fit to the distribution of the invariant mass $M(K^\mp \pi^\pm)$. The fraction of nonprompt D^0 mesons originating from b -hadron decays, called D^0 -from- b in the following, is determined from the $\log_{10}(\chi_{\text{IP}}^2(D^0))$ distribution, where $\chi_{\text{IP}}^2(D^0)$ is defined as the difference in vertex-fit χ^2 of a given PV computed with and without the D^0 meson candidate [51, 52]. On average, prompt D^0 mesons have much smaller $\chi_{\text{IP}}^2(D^0)$ values than D^0 -from- b . The fit is performed in two steps. First, the invariant mass distributions are fitted to determine the D^0 meson inclusive yield and the number of background candidates, then the $\log_{10}(\chi_{\text{IP}}^2(D^0))$ fit is

¹Charge conjugation is implied throughout this document if not otherwise specified.

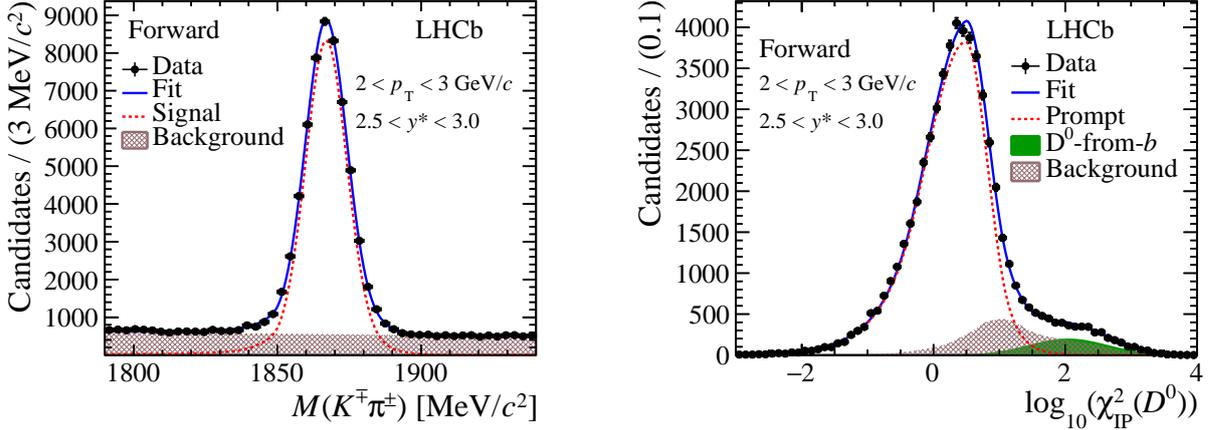


Figure 1: The (left) $M(K^\mp\pi^\pm)$ and (right) $\log_{10}(\chi_{\text{IP}}^2(D^0))$ distributions and the fit result for the inclusive D^0 mesons in the forward data sample in the kinematic range of $2 < p_{\text{T}} < 3 \text{ GeV}/c$ and $2.5 < y^* < 3.0$.

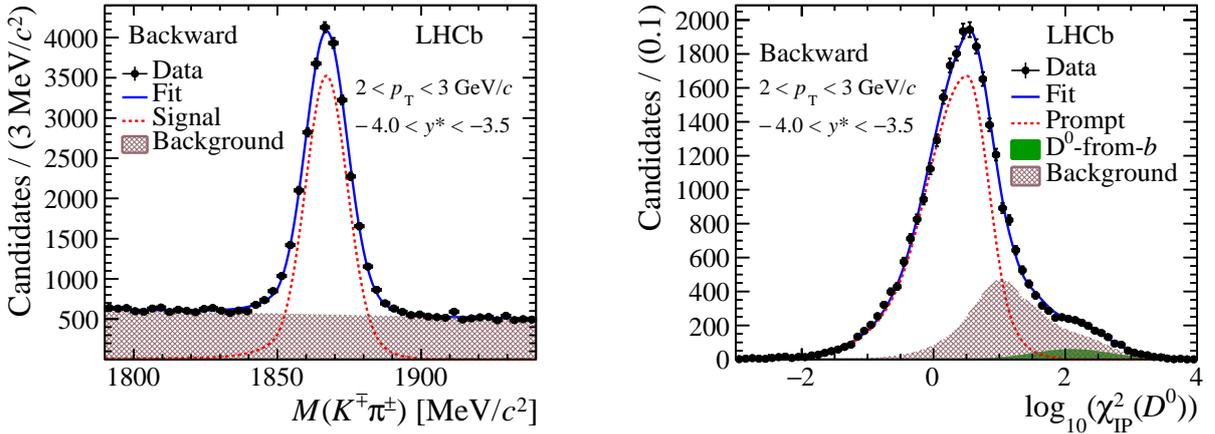


Figure 2: The (left) $M(K^\mp\pi^\pm)$ and (right) $\log_{10}(\chi_{\text{IP}}^2(D^0))$ distributions and the fit result for the inclusive D^0 mesons in the backward data sample in the kinematic range of $2 < p_{\text{T}} < 3 \text{ GeV}/c$ and $-4.0 < y^* < -3.5$.

performed for candidates with mass within $\pm 20 \text{ MeV}/c^2$ around the fitted value of the D^0 mass. In the $\log_{10}(\chi_{\text{IP}}^2(D^0))$ fit, the number of background candidates is constrained to the value obtained from the invariant mass fit, scaled to the selected mass range.

The distribution of $\log_{10}(\chi_{\text{IP}}^2(D^0))$ is shown in the right-hand plots of Figs. 1 and 2 for the forward and backward samples, respectively. The signal shape in the $M(K^\mp\pi^\pm)$ distributions is described by a Crystal Ball (CB) function [53] plus a Gaussian. The mean is the same for both functions, and the ratios of widths and tail parameters are fixed following simulation studies, as in previous LHCb analyses [51, 52]. The width, mean, and signal yields are left free to vary. The background is described by a linear function. The candidates are fitted in the range 1792–1942 MeV/c^2 . The invariant mass distributions in the inclusive forward and backward samples are shown in the left-hand plots of Figs. 1 and 2 respectively.

The fits to the invariant mass and $\log_{10}(\chi_{\text{IP}}^2(D^0))$ distributions are performed independently in each bin of (p_{T}, y^*) of the D^0 meson. The contribution of the D^0 -from- b component increases with transverse momentum up to 10%. The $\log_{10}(\chi_{\text{IP}}^2(D^0))$ shapes for the prompt D^0 meson signal candidates are estimated using the simulation and modelled with a modified Gaussian function

$$f(x; \mu, \sigma, \epsilon, \rho_{\text{L}}, \rho_{\text{R}}) = \begin{cases} e^{\frac{\rho_{\text{L}}^2}{2} + \rho_{\text{L}} \frac{x-\mu}{(1-\epsilon)\sigma}} & x < \mu - (\rho_{\text{L}}\sigma(1-\epsilon)), \\ e^{-\left(\frac{x-\mu}{\sqrt{2}\sigma(1-\epsilon)}\right)^2} & \mu - (\rho_{\text{L}}\sigma(1-\epsilon)) \leq x < \mu, \\ e^{-\left(\frac{x-\mu}{\sqrt{2}\sigma(1+\epsilon)}\right)^2} & \mu \leq x < \mu + (\rho_{\text{R}}\sigma(1+\epsilon)), \\ e^{\frac{\rho_{\text{R}}^2}{2} - \rho_{\text{R}} \frac{x-\mu}{(1+\epsilon)\sigma}} & x \geq \mu + (\rho_{\text{R}}\sigma(1+\epsilon)), \end{cases} \quad (4)$$

where the values of ϵ , ρ_{L} and ρ_{R} are fixed to the values obtained in the simulation and μ and σ are free parameters. The $\log_{10}(\chi_{\text{IP}}^2(D^0))$ distribution for the D^0 -from- b component is described by a Gaussian function. The shape of the combinatorial background is estimated using the distribution of candidates with mass in the ranges 1797–1827 MeV/ c^2 and 1907–1937 MeV/ c^2 , *i.e.* between 40 and 70 MeV/ c^2 away from the observed D^0 meson mass.

The total efficiency ε_{tot} in Eq. 1 includes the effects of geometrical acceptance and the efficiencies of the trigger, of the reconstruction and of the PID criteria used in the analysis. The analysis uses a minimum activity trigger, whose efficiency for events containing a D^0 meson is found to be 100%. The geometrical acceptance and reconstruction efficiencies are estimated using pp simulated samples, validated with data. The difference between the distributions of the track multiplicity in the $p\text{Pb}$ and pp collisions is accounted for by studying the efficiency in bins of the track multiplicity, and weighting the efficiency according to the multiplicity distributions seen in $p\text{Pb}$ and $\text{Pb}p$ data. The related systematic uncertainties are discussed in Sec. 4. The PID efficiency is estimated using a calibration sample of D^0 meson decays selected in data without PID requirements [41], and collected in the same period as the $p\text{Pb}$ sample used for the analysis. The PID selection efficiency is calculated by using the K^{\mp} and π^{\pm} single-track efficiencies from calibration data, and averaging them according to the kinematic distributions observed in the simulation in each D^0 (p_{T}, y^*) bin.

4 Systematic Uncertainties

The systematic uncertainties affecting the cross-sections are listed in Table 1. They are evaluated separately for the backward and forward samples unless otherwise specified. The systematic uncertainty associated to the determination of the signal yield has contributions from the signal and background models. The uncertainty associated to the modelling of the signal is studied by using alternative models of single or sum of two Gaussian functions to fit the invariant mass in the forward and backward samples. A variation of the parameters which are fixed in the default model, within the ranges indicated by the simulation, is also explored. The largest difference between the nominal and the alternative fits is taken as the uncertainty on the method, which results in a bin-dependent uncertainty, not exceeding 5%. The effect due to background modelling in the invariant mass fit is studied by using an exponential as an alternative to the linear

Table 1: Summary of systematic and statistical uncertainties on the cross-section. The ranges indicate the variations between bins, with the uncertainty on average increasing with rapidity and momentum.

Source	Relative uncertainty (%)	
	Forward	Backward
<i>Correlated between bins</i>		
Invariant mass fits	0.0 – 5.0	0.0 – 5.0
$\log_{10}(\chi_{\text{IP}}^2(D^0))$ fits	0.0 – 5.0	0.0 – 5.0
Tracking efficiency	3.0	5.0
PID efficiency	0.6 – 17.0	0.6 – 30.0
Luminosity	1.9	2.1
$\mathcal{B}(D^0 \rightarrow K^\mp \pi^\pm)$	1.0	1.0
<i>Uncorrelated between bins</i>		
Simulation sample size	1.0 – 4.0	1.0 – 5.0
Statistical uncertainty	0.5 – 20.0	1.0 – 20.0

function. This uncertainty is found to be negligible. For the fit to the $\log_{10}(\chi_{\text{IP}}^2(D^0))$ distribution, the ρ_L and ρ_R parameters of the prompt signal component are varied within the ranges studied in simulation. The distribution of combinatorial backgrounds is studied with candidates in different background mass regions. The shape of the distribution for the D^0 -from- b component is fixed when studying the variation of its fraction. The same procedure is followed to estimate the uncertainty on the $\log_{10}(\chi_{\text{IP}}^2(D^0))$ fits. The systematic uncertainty on the prompt signal yields, determined by the $\log_{10}(\chi_{\text{IP}}^2(D^0))$ fit, depends on the kinematic bin and is estimated to be less than 5% in all cases.

The systematic uncertainty associated with the tracking efficiency has the components described in the following. The efficiency measurement is affected by the imperfect modelling of the tracking efficiency by simulation, which is corrected using a data-driven method [54], and the uncertainty of the correction is propagated into an uncertainty on the D^0 yield. The limited sizes of the simulated samples affect the precision of the efficiency, especially in the high multiplicity region. Another source of uncertainty is introduced by the choice of variable representing the detector occupancy, used to weight the distributions. The number of tracks and the number of hits in the VELO and in the TT and OT are all considered separately. The largest difference between the efficiencies when weighted by each of these variables and their average, which is the default, is taken as systematic uncertainty. An additional uncertainty comes from the detector occupancy distribution estimated in backward and forward data. The effects are summed in quadrature, yielding a total uncertainty on the tracking efficiency of 3% and 5% for the forward and backward collision sample respectively.

The limited size of the calibration sample, the binning scheme and the signal fit model used to determine the π and K PID efficiency from the calibration sample, all contribute to the systematic uncertainty. The first is evaluated by estimating new sets of efficiencies through the variation of the π and K PID efficiencies in the calibration sample within the statistical uncertainties, the second by using alternative binning schemes and the third by varying the signal function used to determine the signal. The uncertainty is taken to be the quadratic sum of the three components. The total PID systematic uncertainty ranges

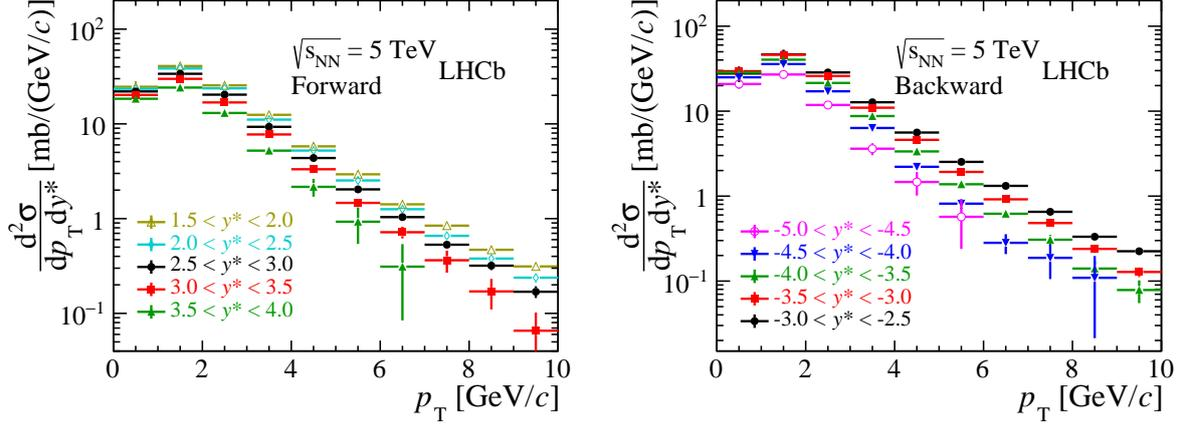


Figure 3: Double-differential cross-section $\frac{d^2\sigma}{dp_T dy^*}$ (mb/(GeV/c)) of prompt D^0 meson production in p Pb collisions in the (left) forward and (right) backward collision samples. The uncertainty is the quadratic sum of the statistical and systematic components.

between 1% and 30% depending on the kinematic region and the collision sample.

The relative uncertainty associated with the luminosity measurement is approximately 2% for both forward and backward samples. The relative uncertainty of the branching fraction $\mathcal{B}(D^0 \rightarrow K^\mp \pi^\pm)$ is 1% [50]. The limited size of the simulation sample introduces uncertainties on the efficiencies which are then propagated to the cross-section measurements; this effect is negligible for the central rapidity region but increases in the regions close to the boundaries of p_T and y , ranging between 1% and 5%.

5 Results

5.1 Production cross-sections

The measured values of the double-differential cross-section of prompt D^0 mesons in proton-lead collisions in the forward and backward regions as a function of p_T and y^* are given in Table 2 and shown in Fig. 3. The one-dimensional differential prompt D^0 meson cross-sections as a function of p_T or y^* are reported in Tables 3 and 4, and are displayed in Fig. 4. The measurements are also shown as a function of p_T integrated² over y^* in the common rapidity range $2.5 < |y^*| < 4.0$.

The integrated cross-sections of prompt D^0 meson production in p Pb forward data in the full and common fiducial regions are

$$\sigma_{\text{forward}}(p_T < 10 \text{ GeV}/c, 1.5 < y^* < 4.0) = 230.6 \pm 0.5 \pm 13.0 \text{ mb},$$

$$\sigma_{\text{forward}}(p_T < 10 \text{ GeV}/c, 2.5 < y^* < 4.0) = 119.1 \pm 0.3 \pm 5.6 \text{ mb}.$$

The integrated cross-sections of prompt D^0 meson production in Pb p backward data in the two fiducial regions are

$$\sigma_{\text{backward}}(p_T < 10 \text{ GeV}/c, -2.5 < y^* < -5.0) = 252.7 \pm 1.0 \pm 20.0 \text{ mb},$$

² The integration over y^* is performed up to $|y^*|=3.5$ for $p_T > 6 \text{ GeV}/c$, neglecting the bin $3.5 < |y^*| < 4.0$ since it is not populated in the forward sample. This applies for the integrated cross-sections presented in this subsection, in Tables 3, 5 and 7 and in Figs. 4, 5, 8 and 9.

Table 2: Double-differential cross-section $\frac{d^2\sigma}{dp_T dy^*}$ (mb/(GeV/c)) for prompt D^0 meson production as functions of p_T and y^* in p Pb forward and backward data, respectively. The first uncertainty is statistical, the second is the component of the systematic uncertainty that is uncorrelated between bins and the third is the correlated component. In the regions with no entries the signal is not statistically significant.

p_T [GeV/c]	Forward (mb/(GeV/c))					
	$1.5 < y^* < 2.0$	$2.0 < y^* < 2.5$	$2.5 < y^* < 3.0$	$3.0 < y^* < 3.5$	$3.5 < y^* < 4.0$	
[0, 1]	24.67 ± 0.32 ± 0.50 ± 3.45	23.48 ± 0.17 ± 0.25 ± 1.70	22.01 ± 0.16 ± 0.20 ± 1.16	20.19 ± 0.21 ± 0.23 ± 1.02	18.41 ± 0.36 ± 0.33 ± 1.09	
[1, 2]	40.79 ± 0.34 ± 0.61 ± 3.83	38.45 ± 0.19 ± 0.35 ± 2.19	33.79 ± 0.18 ± 0.26 ± 1.50	29.89 ± 0.22 ± 0.28 ± 1.31	24.17 ± 0.34 ± 0.40 ± 1.63	
[2, 3]	25.50 ± 0.20 ± 0.39 ± 1.76	23.73 ± 0.11 ± 0.20 ± 1.08	20.34 ± 0.10 ± 0.16 ± 0.82	16.84 ± 0.11 ± 0.17 ± 0.69	13.03 ± 0.17 ± 0.23 ± 0.78	
[3, 4]	12.46 ± 0.11 ± 0.21 ± 0.63	11.09 ± 0.06 ± 0.10 ± 0.47	9.31 ± 0.05 ± 0.09 ± 0.38	7.73 ± 0.06 ± 0.09 ± 0.36	5.22 ± 0.09 ± 0.11 ± 0.46	
[4, 5]	5.79 ± 0.06 ± 0.11 ± 0.27	5.23 ± 0.04 ± 0.06 ± 0.21	4.36 ± 0.03 ± 0.05 ± 0.17	3.32 ± 0.04 ± 0.05 ± 0.14	2.17 ± 0.07 ± 0.07 ± 0.45	
[5, 6]	2.94 ± 0.04 ± 0.07 ± 0.14	2.53 ± 0.03 ± 0.04 ± 0.11	2.04 ± 0.02 ± 0.03 ± 0.09	1.47 ± 0.02 ± 0.03 ± 0.10	0.93 ± 0.07 ± 0.07 ± 0.37	
[6, 7]	1.42 ± 0.02 ± 0.04 ± 0.08	1.26 ± 0.02 ± 0.02 ± 0.05	1.04 ± 0.02 ± 0.02 ± 0.06	0.72 ± 0.02 ± 0.02 ± 0.10	0.31 ± 0.08 ± 0.06 ± 0.20	
[7, 8]	0.84 ± 0.02 ± 0.03 ± 0.04	0.66 ± 0.01 ± 0.02 ± 0.04	0.53 ± 0.01 ± 0.01 ± 0.03	0.36 ± 0.02 ± 0.02 ± 0.09	—	
[8, 9]	0.47 ± 0.01 ± 0.02 ± 0.02	0.38 ± 0.01 ± 0.01 ± 0.03	0.32 ± 0.01 ± 0.01 ± 0.03	0.17 ± 0.02 ± 0.02 ± 0.06	—	
[9, 10]	0.31 ± 0.01 ± 0.02 ± 0.02	0.24 ± 0.01 ± 0.01 ± 0.02	0.17 ± 0.01 ± 0.01 ± 0.02	0.07 ± 0.01 ± 0.01 ± 0.03	—	
p_T [GeV/c]	Backward (mb/(GeV/c))					
	$-3.0 < y^* < -2.5$	$-3.5 < y^* < -3.0$	$-4.0 < y^* < -3.5$	$-4.5 < y^* < -4.0$	$-5.0 < y^* < -4.5$	
[0, 1]	27.75 ± 0.48 ± 0.47 ± 5.78	29.56 ± 0.33 ± 0.29 ± 2.98	28.47 ± 0.38 ± 0.28 ± 1.98	25.03 ± 0.58 ± 0.28 ± 1.78	20.85 ± 1.08 ± 0.43 ± 2.21	
[1, 2]	46.66 ± 0.51 ± 0.69 ± 6.13	46.10 ± 0.35 ± 0.38 ± 3.40	40.35 ± 0.38 ± 0.33 ± 2.61	35.82 ± 0.56 ± 0.38 ± 2.54	27.00 ± 1.01 ± 0.45 ± 2.81	
[2, 3]	28.55 ± 0.29 ± 0.41 ± 2.41	25.90 ± 0.19 ± 0.22 ± 1.62	21.47 ± 0.18 ± 0.17 ± 1.26	17.13 ± 0.23 ± 0.19 ± 1.09	11.82 ± 0.45 ± 0.23 ± 0.97	
[3, 4]	12.73 ± 0.15 ± 0.18 ± 0.93	10.98 ± 0.10 ± 0.10 ± 0.64	8.75 ± 0.09 ± 0.08 ± 0.50	6.33 ± 0.10 ± 0.08 ± 0.45	3.61 ± 0.17 ± 0.09 ± 0.55	
[4, 5]	5.60 ± 0.08 ± 0.09 ± 0.38	4.59 ± 0.05 ± 0.05 ± 0.26	3.36 ± 0.05 ± 0.04 ± 0.19	2.21 ± 0.05 ± 0.03 ± 0.14	1.47 ± 0.13 ± 0.06 ± 0.43	
[5, 6]	2.53 ± 0.05 ± 0.05 ± 0.16	1.93 ± 0.03 ± 0.03 ± 0.11	1.38 ± 0.03 ± 0.02 ± 0.08	0.82 ± 0.03 ± 0.02 ± 0.10	0.57 ± 0.14 ± 0.06 ± 0.30	
[6, 7]	1.32 ± 0.03 ± 0.03 ± 0.08	0.92 ± 0.02 ± 0.02 ± 0.06	0.62 ± 0.02 ± 0.01 ± 0.04	0.28 ± 0.02 ± 0.01 ± 0.07	—	
[7, 8]	0.65 ± 0.02 ± 0.02 ± 0.04	0.48 ± 0.02 ± 0.01 ± 0.04	0.31 ± 0.01 ± 0.01 ± 0.04	0.19 ± 0.03 ± 0.01 ± 0.08	—	
[8, 9]	0.33 ± 0.02 ± 0.01 ± 0.02	0.24 ± 0.01 ± 0.01 ± 0.02	0.14 ± 0.01 ± 0.01 ± 0.03	0.11 ± 0.03 ± 0.01 ± 0.08	—	
[9, 10]	0.22 ± 0.01 ± 0.01 ± 0.02	0.13 ± 0.01 ± 0.01 ± 0.01	0.08 ± 0.01 ± 0.00 ± 0.02	—	—	

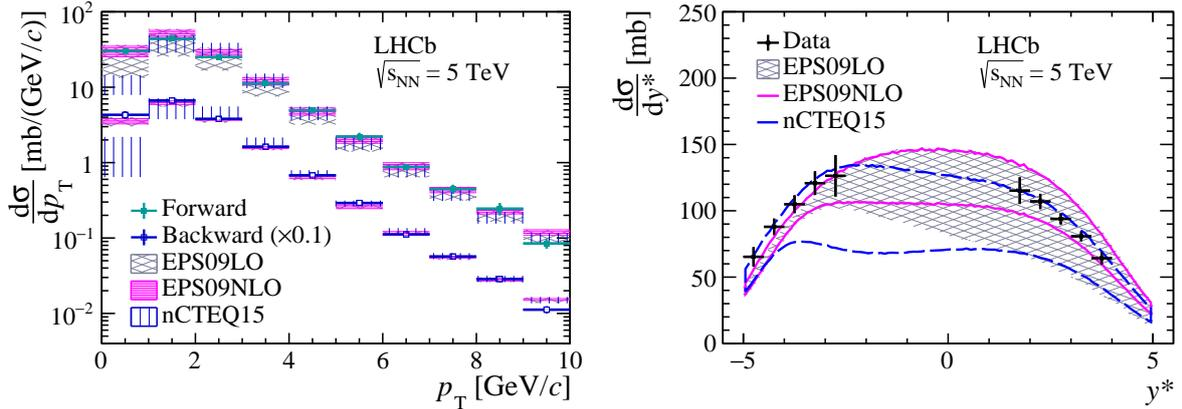


Figure 4: Differential cross-section of prompt D^0 meson production in $p\text{Pb}$ collisions as a function of (left) p_T ($\frac{d\sigma}{dp_T}$) and (right) y^* ($\frac{d\sigma}{dy^*}$) in the forward and backward collision samples. The uncertainty is the quadratic sum of the statistical and systematic components. The measurements are compared with theoretical predictions including different nuclear parton distribution functions as explained in the text.

$$\sigma_{\text{backward}}(p_T < 10 \text{ GeV}/c, -2.5 < y^* < -4.0) = 175.5 \pm 0.6 \pm 14.4 \text{ mb},$$

where the first uncertainties are statistical and the second systematic.

The cross-sections as a function of p_T and y^* , shown in Fig. 4, are compared with calculations [55–57] validated with results of heavy-flavour production cross-section in pp collisions. The nuclear effects are considered by using three different sets of nuclear parton distribution functions (nPDFs), the leading-order EPS09 (EPS09LO) [58], the next-to-leading order EPS09 (EPS09NLO) [58] and nCTEQ15 [59]. The free nucleon PDF CT10NLO [60] is also used as a reference for the cross-section predictions in pp collisions. Within large theoretical uncertainties, all three sets of nPDFs can give descriptions consistent with the LHCb data, although a discrepancy is observed in the low p_T region between the measurements and the nCTEQ15 predictions.

5.2 Nuclear modification factors

The value of the D^0 meson production cross-section in pp collisions at 5 TeV, needed for the measurement of the nuclear modification factor $R_{p\text{Pb}}$, is taken from the LHCb measurement [61]. Correlations between the uncertainties of quantities that are common to both measurements are taken into account. The nuclear modification factor for prompt D^0 meson production is shown in Fig. 5 in bins of p_T and Fig. 6 in bins of y^* . The nuclear modification factors are calculated as a function of p_T integrated over y^* in the ranges described in Fig. 5 for both forward and backward samples. The values of $R_{p\text{Pb}}$, summarised in Tables 5 and 6, show a slight increase as a function of p_T , suggesting that the suppression may decrease with increasing transverse momentum.

The measurements are compared with calculations using EPS09LO, EPSNLO and nCTEQ15 nPDFs [55–57]. For the results in the backward configuration, all three predictions show reasonable agreement with each other and with LHCb data. In the forward configuration, nCTEQ15 and EPS09LO show better agreement with the data than EPS09NLO. Calculations [62] using CTEQ6M [63] nucleon PDF and EPS09NLO nPDF

Table 3: Measured differential cross-section $\frac{d\sigma}{dp_T}$ (mb/(GeV/c)) for prompt D^0 meson production as a function of p_T in p Pb forward and backward data, respectively. The first uncertainty is statistical, the second is the component of the systematic uncertainty that is uncorrelated between bins and the third is the correlated component. The results in the last two columns are integrated over the common rapidity range $2.5 < |y^*| < 4.0$ for $p_T < 6$ GeV/c and over $2.5 < |y^*| < 3.5$ for $6 < p_T < 10$ GeV/c.

p_T [GeV/c]	Forward (mb/(GeV/c))		
	$1.5 < y^* < 4.0$	$2.5 < y^* < 4.0$	$2.5 < y^* < 3.5$
[0, 1]	$54.38 \pm 0.29 \pm 0.36 \pm 3.96$	$30.31 \pm 0.22 \pm 0.22 \pm 1.59$	—
[1, 2]	$83.54 \pm 0.30 \pm 0.45 \pm 5.01$	$43.92 \pm 0.22 \pm 0.28 \pm 2.17$	—
[2, 3]	$49.72 \pm 0.16 \pm 0.27 \pm 2.45$	$25.11 \pm 0.11 \pm 0.16 \pm 1.11$	—
[3, 4]	$22.91 \pm 0.09 \pm 0.14 \pm 1.10$	$11.13 \pm 0.06 \pm 0.08 \pm 0.55$	—
[4, 5]	$10.43 \pm 0.06 \pm 0.08 \pm 0.54$	$4.92 \pm 0.04 \pm 0.05 \pm 0.32$	—
[5, 6]	$4.95 \pm 0.05 \pm 0.06 \pm 0.35$	$2.21 \pm 0.04 \pm 0.04 \pm 0.26$	—
[6, 7]	$2.37 \pm 0.05 \pm 0.04 \pm 0.21$	—	$0.88 \pm 0.01 \pm 0.01 \pm 0.07$
[7, 8]	$1.20 \pm 0.02 \pm 0.02 \pm 0.09$	—	$0.45 \pm 0.01 \pm 0.01 \pm 0.06$
[8, 9]	$0.67 \pm 0.01 \pm 0.01 \pm 0.06$	—	$0.24 \pm 0.01 \pm 0.01 \pm 0.04$
[9, 10]	$0.39 \pm 0.01 \pm 0.01 \pm 0.04$	—	$0.08 \pm 0.00 \pm 0.00 \pm 0.01$
p_T [GeV/c]	Backward (mb/(GeV/c))		
	$-5.0 < y^* < -2.5$	$-4.0 < y^* < -2.5$	$-3.5 < y^* < -2.5$
[0, 1]	$65.83 \pm 0.70 \pm 0.40 \pm 6.85$	$42.89 \pm 0.35 \pm 0.31 \pm 5.15$	—
[1, 2]	$97.97 \pm 0.68 \pm 0.52 \pm 8.30$	$66.56 \pm 0.36 \pm 0.43 \pm 5.80$	—
[2, 3]	$52.43 \pm 0.32 \pm 0.29 \pm 3.57$	$37.96 \pm 0.20 \pm 0.25 \pm 2.56$	—
[3, 4]	$21.21 \pm 0.14 \pm 0.13 \pm 1.45$	$16.23 \pm 0.10 \pm 0.11 \pm 1.01$	—
[4, 5]	$8.62 \pm 0.09 \pm 0.06 \pm 0.62$	$6.78 \pm 0.05 \pm 0.05 \pm 0.41$	—
[5, 6]	$3.61 \pm 0.08 \pm 0.04 \pm 0.33$	$2.92 \pm 0.03 \pm 0.03 \pm 0.18$	—
[6, 7]	$1.57 \pm 0.03 \pm 0.02 \pm 0.12$	—	$1.12 \pm 0.02 \pm 0.02 \pm 0.07$
[7, 8]	$0.81 \pm 0.02 \pm 0.01 \pm 0.09$	—	$0.57 \pm 0.01 \pm 0.01 \pm 0.04$
[8, 9]	$0.41 \pm 0.02 \pm 0.01 \pm 0.07$	—	$0.29 \pm 0.01 \pm 0.01 \pm 0.02$
[9, 10]	$0.22 \pm 0.01 \pm 0.01 \pm 0.02$	—	$0.11 \pm 0.01 \pm 0.01 \pm 0.01$

give results for R_{pPb} that are similar to a combination of CT10NLO and EPS09NLO.

The nuclear modification factors for prompt D^0 are also compared with those for prompt J/ψ [43] in Fig. 6 as a function of p_T integrated over rapidity, and they are found to be consistent. This is the first measurement of R_{pPb} in this kinematic range. The ratios of the nuclear modification factors of J/ψ and $\psi(2S)$ mesons to D^0 mesons as a function of rapidity are shown in Fig. 7 where a different suppression between the two charmonium states can be observed. In Figs. 5 and 6 the measurements are also compared with calculations in the colour glass condensate framework (CGC) [64], which includes the effect of the saturation of partons at small x . The CGC model is found to be able to describe the trend of prompt D^0 meson nuclear modifications as a function of p_T and of rapidity. The uncertainty band for this model is much smaller than for the nuclear PDF calculations, since it only contains the variation of charm quark masses and factorisation scale which largely cancel in this ratio of cross-sections. Another CGC framework calculation gives similar results for nuclear modifications of charm production [65]. In the context of p Pb collisions, recent measurements have shown that long-range collective effects, which have previously been observed in relatively large nucleus-nucleus collision systems, may also be present in smaller collision systems at large charged particle multiplicities [66–69]. If these

Table 4: Differential cross-section $\frac{d\sigma}{dy^*}$ (mb) for prompt D^0 meson production as a function of $|y^*|$ in p Pb forward and backward data, respectively. The first uncertainty is statistical, the second is the component of the systematic uncertainty that is uncorrelated between bins and the third is the correlated component.

Forward (mb)	
y^*	$0 < p_T < 10 \text{ GeV}/c$
[1.5, 2.0]	$115.19 \pm 0.53 \pm 0.91 \pm 9.99$
[2.0, 2.5]	$107.05 \pm 0.29 \pm 0.50 \pm 5.73$
[2.5, 3.0]	$93.90 \pm 0.27 \pm 0.38 \pm 4.14$
[3.0, 3.5]	$80.76 \pm 0.33 \pm 0.42 \pm 3.71$
[3.5, 4.0]	$64.24 \pm 0.55 \pm 0.58 \pm 4.79$
Backward (mb)	
y^*	$0 < p_T < 10 \text{ GeV}/c$
[-3.0, -2.5]	$126.35 \pm 0.78 \pm 0.95 \pm 15.54$
[-3.5, -3.0]	$120.84 \pm 0.53 \pm 0.53 \pm 8.89$
[-4.0, -3.5]	$104.93 \pm 0.58 \pm 0.47 \pm 6.66$
[-4.5, -4.0]	$87.92 \pm 0.85 \pm 0.52 \pm 6.13$
[-5.0, -4.5]	$65.32 \pm 1.57 \pm 0.68 \pm 7.07$

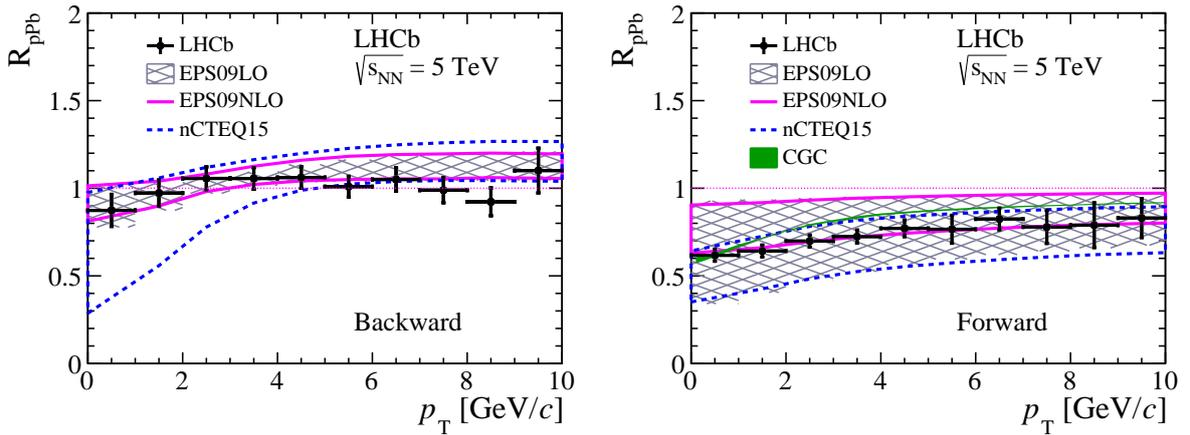


Figure 5: Nuclear modification factor R_{pPb} as a function of p_T for prompt D^0 meson production in the (left) backward data and (right) forward data, integrated over the common rapidity range $2.5 < |y^*| < 4.0$ for $p_T < 6 \text{ GeV}/c$ and over $2.5 < |y^*| < 3.5$ for $6 < p_T < 10 \text{ GeV}/c$. The uncertainty is the quadratic sum of the statistical and systematic components. The CGC predictions are only available for the forward region.

effects are due to the creation of a hydrodynamic system, momentum anisotropies at the quark level can arise, which may modify the final distribution of observed heavy-quark hadrons [70]. Since the measurements in this analysis do not consider a classification in charged particle multiplicity, potential modifications in high-multiplicity events are weakened as the presented observables are integrated over charged particle multiplicity.

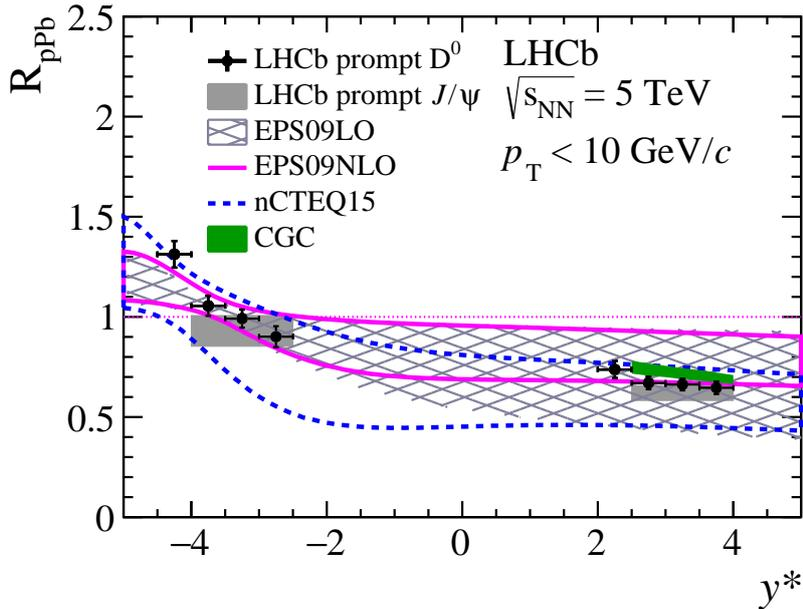


Figure 6: Nuclear modification factor R_{pPb} as a function of y^* for prompt D^0 meson production, integrated up to $p_T = 10$ GeV/c. The uncertainty is the quadratic sum of the statistical and systematic components.

Table 5: Nuclear modification factor R_{pPb} for prompt D^0 meson production in different p_T ranges, integrated over the common rapidity range $2.5 < |y^*| < 4.0$ for $p_T < 6$ GeV/c and over $2.5 < |y^*| < 3.5$ for $6 < p_T < 10$ GeV/c for the forward (positive y^*) and backward (negative y^*) samples. The first uncertainty is statistical and the second systematic.

p_T [GeV/c]	Forward	Backward
[0, 1]	$0.62 \pm 0.01 \pm 0.03$	$0.87 \pm 0.01 \pm 0.09$
[1, 2]	$0.64 \pm 0.01 \pm 0.03$	$0.97 \pm 0.01 \pm 0.07$
[2, 3]	$0.70 \pm 0.01 \pm 0.03$	$1.06 \pm 0.01 \pm 0.07$
[3, 4]	$0.72 \pm 0.01 \pm 0.04$	$1.06 \pm 0.01 \pm 0.06$
[4, 5]	$0.77 \pm 0.01 \pm 0.05$	$1.06 \pm 0.01 \pm 0.06$
[5, 6]	$0.77 \pm 0.02 \pm 0.08$	$1.01 \pm 0.02 \pm 0.06$
[6, 7]	$0.82 \pm 0.02 \pm 0.06$	$1.05 \pm 0.03 \pm 0.06$
[7, 8]	$0.78 \pm 0.03 \pm 0.09$	$0.99 \pm 0.04 \pm 0.06$
[8, 9]	$0.79 \pm 0.05 \pm 0.12$	$0.92 \pm 0.05 \pm 0.07$
[9, 10]	$0.83 \pm 0.07 \pm 0.09$	$1.10 \pm 0.10 \pm 0.09$
[0, 10]	$0.66 \pm 0.00 \pm 0.03$	$0.97 \pm 0.01 \pm 0.07$

5.3 Forward-backward ratio

In the forward-backward production ratio R_{FB} the common uncertainty between the forward and backward measurements largely cancels. The uncertainties of branching fraction, signal yield and tracking are considered fully correlated, while the PID uncertainty is considered 90% correlated since it is a mixture of statistical uncertainty (uncorrelated) and the uncertainties due to the binning scheme and yield determination (correlated).

Table 6: Nuclear modification factor $R_{p\text{Pb}}$ for prompt D^0 meson production in different y^* ranges, integrated up to $p_T = 10 \text{ GeV}/c$. The first uncertainty is statistical and the second systematic.

y^*	$R_{p\text{Pb}}$
$[-4.5, -4.0]$	$1.31 \pm 0.02 \pm 0.06$
$[-4.0, -3.5]$	$1.05 \pm 0.01 \pm 0.05$
$[-3.5, -3.0]$	$0.99 \pm 0.01 \pm 0.04$
$[-3.0, -2.5]$	$0.90 \pm 0.01 \pm 0.05$
$[2.0, 2.5]$	$0.74 \pm 0.01 \pm 0.04$
$[2.5, 3.0]$	$0.67 \pm 0.00 \pm 0.03$
$[3.0, 3.5]$	$0.66 \pm 0.00 \pm 0.03$
$[3.5, 4.0]$	$0.65 \pm 0.01 \pm 0.03$

Table 7: Forward-backward ratio R_{FB} for prompt D^0 meson production in different p_T ranges, integrated over the common rapidity range $2.5 < |y^*| < 4.0$ for $p_T < 6 \text{ GeV}/c$ and over $2.5 < |y^*| < 3.5$ for $6 < p_T < 10 \text{ GeV}/c$, and in different y^* ranges integrated up to $p_T = 10 \text{ GeV}/c$. The first uncertainty is the statistical and the second is the systematic component.

$p_T [\text{GeV}/c]$	R_{FB}
$[0, 1]$	$0.71 \pm 0.01 \pm 0.06$
$[1, 2]$	$0.66 \pm 0.00 \pm 0.04$
$[2, 3]$	$0.66 \pm 0.00 \pm 0.03$
$[3, 4]$	$0.69 \pm 0.01 \pm 0.03$
$[4, 5]$	$0.73 \pm 0.01 \pm 0.04$
$[5, 6]$	$0.76 \pm 0.02 \pm 0.08$
$[6, 7]$	$0.79 \pm 0.02 \pm 0.05$
$[7, 8]$	$0.79 \pm 0.03 \pm 0.09$
$[8, 9]$	$0.86 \pm 0.04 \pm 0.12$
$[9, 10]$	$0.75 \pm 0.06 \pm 0.09$
$[0, 10]$	$0.68 \pm 0.00 \pm 0.04$
$ y^* $	R_{FB}
$[2.5, 3.0]$	$0.74 \pm 0.01 \pm 0.07$
$[3.0, 3.5]$	$0.67 \pm 0.00 \pm 0.03$
$[3.5, 4.0]$	$0.61 \pm 0.01 \pm 0.03$

All other uncertainties are uncorrelated. The measured R_{FB} values are shown in Fig. 8, as a function of p_T integrated over the range $2.5 < |y^*| < 4.0$, and as a function of y^* integrated up to $p_T = 10 \text{ GeV}/c$. The R_{FB} values in different kinematic bins are also summarised in Table 7. Good agreement is found between measurements and theoretical predictions using EPS09LO and nCTEQ15 nPDFs.

In the common kinematic range $p_T < 10 \text{ GeV}/c$, $2.5 < |y^*| < 4.0$, the forward-backward ratio R_{FB} is $0.71 \pm 0.01(\text{stat}) \pm 0.04(\text{syst})$, indicating a significant asymmetry. The predictions for R_{FB} integrated over the same kinematic range are $0.71_{-0.24}^{+0.21}$ for EPS09 at leading order, $0.81_{-0.09}^{+0.10}$ for EPS09 at next-to-leading order and $0.69_{-0.07}^{+0.07}$ for the nCTEQ15 nPDF set, which are all in good agreement with the measured value. The forward-backward production ratio increases slightly with increasing p_T , and decreases strongly

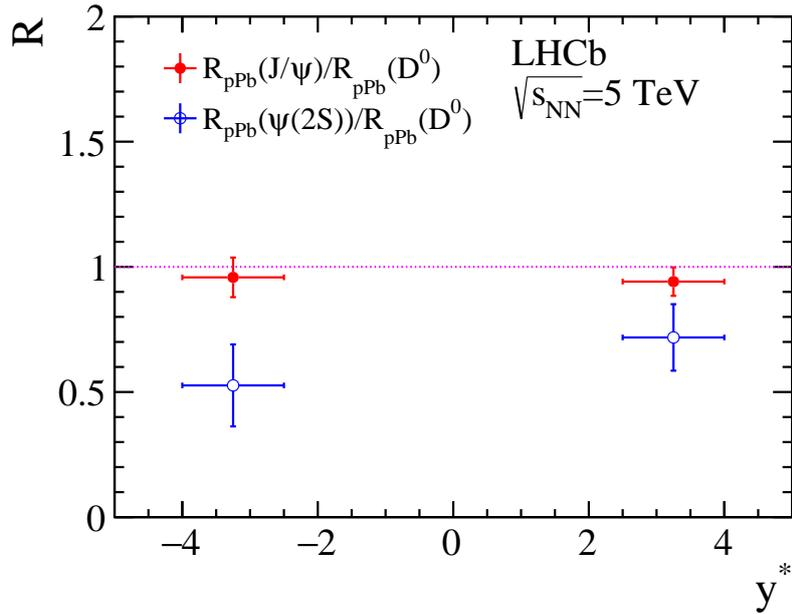


Figure 7: Ratio of nuclear modification factors $R_{p\text{Pb}}$ of J/ψ and $\psi(2S)$ to D^0 mesons in bins of rapidity integrated up to $p_T = 10$ GeV/c in the common rapidity range $2.5 < |y^*| < 4.0$. The uncertainty is the quadratic sum of the statistical and systematic components.

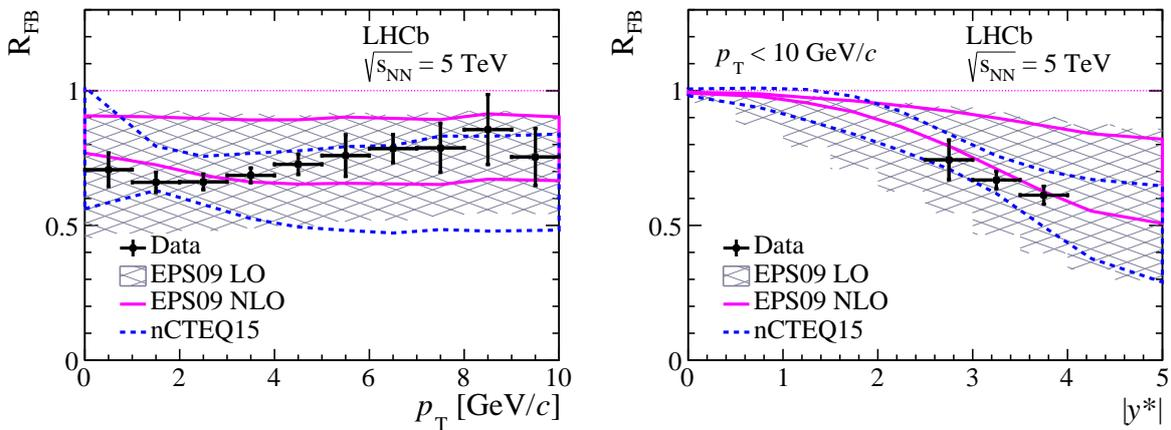


Figure 8: Forward-backward ratio R_{FB} for prompt D^0 meson production (left) as a function of p_T integrated over the common rapidity range $2.5 < |y^*| < 4.0$ for $p_T < 6$ GeV/c and over $2.5 < |y^*| < 3.5$ for $6 < p_T < 10$ GeV/c; (right) as a function of y^* integrated up to $p_T = 10$ GeV/c. The uncertainty is the quadratic sum of the statistical and systematic components.

with increasing rapidity $|y^*|$. This behaviour is consistent with the expectations from the QCD calculations.

In order to compare the production of open charm and charmonium, the ratio of R_{FB} for prompt J/ψ mesons divided by R_{FB} for prompt D^0 mesons is shown in Fig. 9. The measurement shows that R_{FB} has the same size for prompt D^0 and prompt J/ψ mesons within the uncertainties in the LHCb kinematic range.

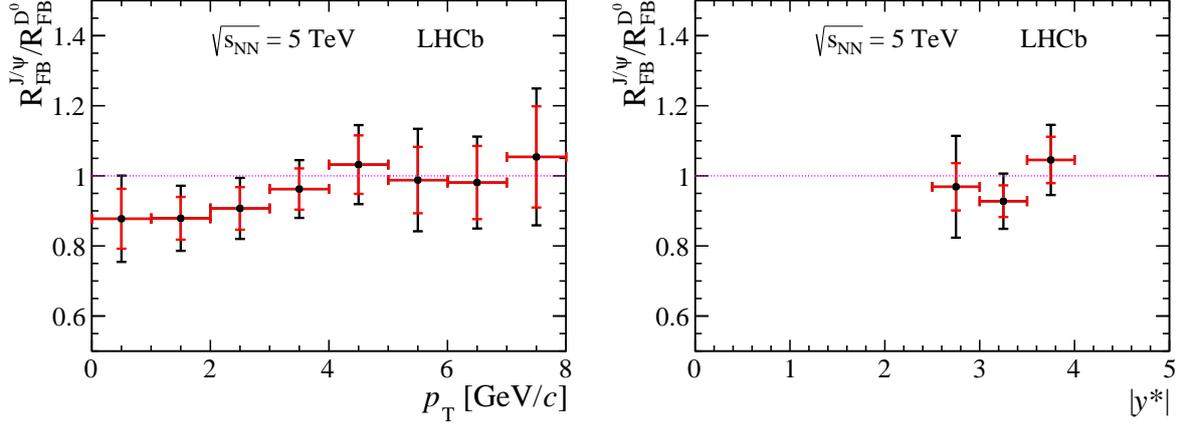


Figure 9: Relative forward-backward production ratio R_{FB} for prompt D^0 mesons over that for prompt J/ψ mesons (left) as a function of p_{T} integrated over the common rapidity range $2.5 < |y^*| < 4.0$ for $p_{\text{T}} < 6 \text{ GeV}/c$ and over $2.5 < |y^*| < 3.5$ for $6 < p_{\text{T}} < 10 \text{ GeV}/c$; (right) as a function of y^* integrated up to $p_{\text{T}} = 10 \text{ GeV}/c$. The red inner bars in the uncertainty represent the statistical uncertainty and the black outer bars the quadratic sum of the statistical and systematic components.

6 Conclusion

The prompt D^0 production cross-section has been measured with LHCb proton-lead collision data at $\sqrt{s_{\text{NN}}} = 5 \text{ TeV}$. The measurement is performed in the range of D^0 transverse momentum $p_{\text{T}} < 10 \text{ GeV}/c$, in both backward and forward collisions covering the ranges $1.5 < y^* < 4.0$ and $-5.0 < y^* < -2.5$. This is the first measurement of this kind down to zero transverse momentum of the D^0 meson. Nuclear modification factors and forward-backward production ratios are also measured in the same kinematic range. Both observables are excellent probes to constrain the PDF uncertainties, which are currently significantly larger than the uncertainties on the experimental results. A large asymmetry in the forward-backward production is observed, which is consistent with the expectations from nuclear parton distribution functions, and colour glass condensate calculations for the forward rapidity part. The results are found to be consistent with the theoretical predictions considered.

Acknowledgements

We would like to thank Andrea Dainese, Bertrand Ducloué, Jean-Philippe Lansberg and Huasheng Shao for providing the theoretical predictions for our measurements. We express our gratitude to our colleagues in the CERN accelerator departments for the excellent performance of the LHC. We thank the technical and administrative staff at the LHCb institutes. We acknowledge support from CERN and from the national agencies: CAPES, CNPq, FAPERJ and FINEP (Brazil); MOST and NSFC (China); CNRS/IN2P3 (France); BMBF, DFG and MPG (Germany); INFN (Italy); NWO (The Netherlands); MNiSW

and NCN (Poland); MEN/IFA (Romania); MinES and FASO (Russia); MinECo (Spain); SNSF and SER (Switzerland); NASU (Ukraine); STFC (United Kingdom); NSF (USA). We acknowledge the computing resources that are provided by CERN, IN2P3 (France), KIT and DESY (Germany), INFN (Italy), SURF (The Netherlands), PIC (Spain), GridPP (United Kingdom), RRCKI and Yandex LLC (Russia), CSCS (Switzerland), IFIN-HH (Romania), CBPF (Brazil), PL-GRID (Poland) and OSC (USA). We are indebted to the communities behind the multiple open source software packages on which we depend. Individual groups or members have received support from AvH Foundation (Germany), EPLANET, Marie Skłodowska-Curie Actions and ERC (European Union), Conseil Général de Haute-Savoie, Labex ENIGMASS and OCEVU, Région Auvergne (France), RFBR and Yandex LLC (Russia), GVA, XuntaGal and GENCAT (Spain), Herchel Smith Fund, The Royal Society, Royal Commission for the Exhibition of 1851 and the Leverhulme Trust (United Kingdom).

References

- [1] B. A. Kniehl, G. Kramer, I. Schienbein, and H. Spiesberger, *Reconciling open charm production at the Fermilab Tevatron with QCD*, Phys. Rev. Lett. **96** (2006) 012001, [arXiv:hep-ph/0508129](#).
- [2] B. A. Kniehl, G. Kramer, I. Schienbein, and H. Spiesberger, *Inclusive charmed-meson production at the CERN LHC*, Eur. Phys. J. **C72** (2012) 2082, [arXiv:1202.0439](#).
- [3] M. Cacciari, M. Greco, and P. Nason, *The p_T spectrum in heavy flavor hadroproduction*, JHEP **05** (1998) 007, [arXiv:hep-ph/9803400](#).
- [4] M. Cacciari and P. Nason, *Charm cross-sections for the Tevatron Run II*, JHEP **09** (2003) 006, [arXiv:hep-ph/0306212](#).
- [5] M. Cacciari *et al.*, *Theoretical predictions for charm and bottom production at the LHC*, JHEP **10** (2012) 137, [arXiv:1205.6344](#).
- [6] R. Maciula and A. Szczurek, *Open charm production at the LHC: k_t -factorization approach*, Phys. Rev. **D87** (2013) 094022, [arXiv:1301.3033](#).
- [7] A. Andronic *et al.*, *Heavy-flavour and quarkonium production in the LHC era: from proton-proton to heavy-ion collisions*, Eur. Phys. J. **C76** (2016) 107, [arXiv:1506.03981](#).
- [8] D. Kharzeev and K. Tuchin, *Signatures of the color glass condensate in J/ψ production off nuclear targets*, Nucl. Phys. **A770** (2006) 40, [arXiv:hep-ph/0510358](#).
- [9] H. Fujii, F. Gelis, and R. Venugopalan, *Quark pair production in high energy pA collisions: General features*, Nucl. Phys. **A780** (2006) 146, [arXiv:hep-ph/0603099](#).
- [10] F. Arleo and S. Peigné, *Heavy-quarkonium suppression in $p-A$ collisions from parton energy loss in cold QCD matter*, JHEP **03** (2013) 122, [arXiv:1212.0434](#).
- [11] S. Gavin and J. Milana, *Energy loss at large x_F in nuclear collisions*, Phys. Rev. Lett. **68** (1992) 1834.

- [12] R. Vogt, *The x_F dependence of ψ and Drell-Yan production*, Phys. Rev. **C61** (2000) 035203, arXiv:hep-ph/9907317.
- [13] N. Armesto, *Nuclear shadowing*, J. Phys. **G32** (2006) R367, arXiv:hep-ph/0604108.
- [14] S. Malace, D. Gaskell, D. W. Higinbotham, and I. Cloet, *The challenge of the EMC effect: Existing data and future directions*, Int. J. Mod. Phys. **E23** (2014) 1430013, arXiv:1405.1270.
- [15] H. Fujii and K. Watanabe, *Heavy quark pair production in high energy pA collisions: Open heavy flavors*, Nucl. Phys. **A920** (2013) 78, arXiv:1308.1258.
- [16] P. Tribedy and R. Venugopalan, *QCD saturation at the LHC: Comparisons of models to $p + p$ and $A + A$ data and predictions for $p + Pb$ collisions*, Phys. Lett. **B710** (2012) 125, arXiv:1112.2445, [Erratum: Phys. Lett. **B718** (2013) 1154].
- [17] J. L. Albacete, A. Dumitru, H. Fujii, and Y. Nara, *CGC predictions for $p + Pb$ collisions at the LHC*, Nucl. Phys. **A897** (2013) 1, arXiv:1209.2001.
- [18] A. H. Rezaeian, *CGC predictions for $p+A$ collisions at the LHC and signature of QCD saturation*, Phys. Lett. **B718** (2013) 1058, arXiv:1210.2385.
- [19] ALICE collaboration, B. Abelev *et al.*, *Suppression of high transverse momentum D mesons in central Pb-Pb collisions at $\sqrt{s_{NN}} = 2.76$ TeV*, JHEP **09** (2012) 112, arXiv:1203.2160.
- [20] R. Averbeck, *Heavy-flavor production in heavy-ion collisions and implications for the properties of hot QCD matter*, Prog. Part. Nucl. Phys. **70** (2013) 159, arXiv:1505.03828.
- [21] ALICE collaboration, D. Adamova *et al.*, *J/ψ production as a function of charged-particle pseudorapidity density in pPb collisions at $\sqrt{s_{NN}} = 5.02$ TeV*, arXiv:1704.00274.
- [22] ALICE collaboration, J. Adam *et al.*, *D -meson production in p -Pb collisions at $\sqrt{s_{NN}} = 5.02$ TeV and in pp collisions at $\sqrt{s} = 7$ TeV*, Phys. Rev. **C94** (2016) 054908, arXiv:1605.07569.
- [23] ALICE collaboration, J. Adam *et al.*, *Centrality dependence of $\psi(2S)$ suppression in p -Pb collisions at $\sqrt{s_{NN}} = 5.02$ TeV*, JHEP **06** (2016) 050, arXiv:1603.02816.
- [24] ALICE collaboration, J. Adam *et al.*, *Measurement of D -meson production versus multiplicity in p -Pb collisions at $\sqrt{s_{NN}} = 5.02$ TeV*, JHEP **08** (2016) 078, arXiv:1602.07240.
- [25] ALICE collaboration, J. Adam *et al.*, *Centrality dependence of inclusive J/ψ production in p -Pb collisions at $\sqrt{s_{NN}} = 5.02$ TeV*, JHEP **11** (2015) 127, arXiv:1506.08808.
- [26] ALICE collaboration, J. Adam *et al.*, *Rapidity and transverse-momentum dependence of the inclusive J/ψ nuclear modification factor in p -Pb collisions at $\sqrt{s_{NN}} = 5.02$ TeV*, JHEP **06** (2015) 055, arXiv:1503.07179.

- [27] ALICE collaboration, B. B. Abelev *et al.*, *Production of inclusive $\Upsilon(1S)$ and $\Upsilon(2S)$ in p -Pb collisions at $\sqrt{s_{\text{NN}}} = 5.02$ TeV*, Phys. Lett. **B740** (2015) 105, [arXiv:1410.2234](#).
- [28] ALICE collaboration, B. B. Abelev *et al.*, *Measurement of prompt D -meson production in p -Pb collisions at $\sqrt{s_{\text{NN}}} = 5.02$ TeV*, Phys. Rev. Lett. **113** (2014) 232301, [arXiv:1405.3452](#).
- [29] ALICE collaboration, B. B. Abelev *et al.*, *J/ψ production and nuclear effects in p -Pb collisions at $\sqrt{s_{\text{NN}}} = 5.02$ TeV*, JHEP **02** (2014) 073, [arXiv:1308.6726](#).
- [30] ALICE collaboration, B. B. Abelev *et al.*, *Suppression of $\psi(2S)$ production in p -Pb collisions at $\sqrt{s_{\text{NN}}} = 5.02$ TeV*, JHEP **12** (2014) 073, [arXiv:1405.3796](#).
- [31] ATLAS collaboration, G. Aad *et al.*, *Measurement of differential J/ψ production cross sections and forward-backward ratios in p Pb collisions with the ATLAS detector*, Phys. Rev. **C92** (2015) 034904, [arXiv:1505.08141](#).
- [32] CMS collaboration, S. Chatrchyan *et al.*, *Event activity dependence of $Y(nS)$ production in $\sqrt{s_{\text{NN}}} = 5.02$ TeV p Pb and $\sqrt{s} = 2.76$ TeV pp collisions*, JHEP **04** (2014) 103, [arXiv:1312.6300](#).
- [33] CMS collaboration, A. M. Sirunyan *et al.*, *Measurement of prompt and nonprompt J/ψ production in pp and p Pb collisions at $\sqrt{s_{\text{NN}}} = 5.02$ TeV*, Eur. Phys. J. **C77** (2017) 269, [arXiv:1702.01462](#).
- [34] CMS collaboration, A. M. Sirunyan *et al.*, *Measurements of the charm jet cross section and nuclear modification factor in p Pb collisions at $\sqrt{s_{\text{NN}}} = 5.02$ TeV*, [arXiv:1612.08972](#).
- [35] CMS collaboration, V. Khachatryan *et al.*, *Transverse momentum spectra of inclusive b jets in p Pb collisions at $\sqrt{s_{\text{NN}}} = 5.02$ TeV*, Phys. Lett. **B754** (2016) 59, [arXiv:1510.03373](#).
- [36] CMS collaboration, V. Khachatryan *et al.*, *Study of B meson production in p Pb collisions at $\sqrt{s_{\text{NN}}} = 5.02$ TeV using exclusive hadronic decays*, Phys. Rev. Lett. **116** (2016) 032301, [arXiv:1508.06678](#).
- [37] ALICE collaboration, J. Adam *et al.*, *Measurement of electrons from heavy-flavour hadron decays in p -Pb collisions at $\sqrt{s_{\text{NN}}} = 5.02$ TeV*, Phys. Lett. **B754** (2016) 81, [arXiv:1509.07491](#).
- [38] ALICE collaboration, J. Adam *et al.*, *Measurement of electrons from beauty-hadron decays in p -Pb collisions at $\sqrt{s_{\text{NN}}} = 5.02$ TeV and Pb-Pb collisions at $\sqrt{s_{\text{NN}}} = 2.76$ TeV*, [arXiv:1609.03898](#).
- [39] ALICE collaboration, S. Acharya *et al.*, *Production of muons from heavy-flavour hadron decays in p -Pb collisions at $\sqrt{s_{\text{NN}}} = 5.02$ TeV*, Phys. Lett. **B770** (2017) 459, [arXiv:1702.01479](#).
- [40] LHCb collaboration, A. A. Alves Jr. *et al.*, *The LHCb detector at the LHC*, JINST **3** (2008) S08005.

- [41] LHCb collaboration, R. Aaij *et al.*, *LHCb detector performance*, Int. J. Mod. Phys. **A30** (2015) 1530022, [arXiv:1412.6352](#).
- [42] R. Aaij *et al.*, *The LHCb trigger and its performance in 2011*, JINST **8** (2013) P04022, [arXiv:1211.3055](#).
- [43] LHCb collaboration, R. Aaij *et al.*, *Study of J/ψ production and cold nuclear matter effects in pPb collisions at $\sqrt{s_{NN}} = 5$ TeV*, JHEP **02** (2014) 072, [arXiv:1308.6729](#).
- [44] T. Sjöstrand, S. Mrenna, and P. Skands, *PYTHIA 6.4 physics and manual*, JHEP **05** (2006) 026, [arXiv:hep-ph/0603175](#); T. Sjöstrand, S. Mrenna, and P. Skands, *A brief introduction to PYTHIA 8.1*, Comput. Phys. Commun. **178** (2008) 852, [arXiv:0710.3820](#).
- [45] I. Belyaev *et al.*, *Handling of the generation of primary events in Gauss, the LHCb simulation framework*, J. Phys. Conf. Ser. **331** (2011) 032047.
- [46] D. J. Lange, *The EvtGen particle decay simulation package*, Nucl. Instrum. Meth. **A462** (2001) 152.
- [47] P. Golonka and Z. Was, *PHOTOS Monte Carlo: A precision tool for QED corrections in Z and W decays*, Eur. Phys. J. **C45** (2006) 97, [arXiv:hep-ph/0506026](#).
- [48] Geant4 collaboration, J. Allison *et al.*, *Geant4 developments and applications*, IEEE Trans. Nucl. Sci. **53** (2006) 270; Geant4 collaboration, S. Agostinelli *et al.*, *Geant4: A simulation toolkit*, Nucl. Instrum. Meth. **A506** (2003) 250.
- [49] M. Clemencic *et al.*, *The LHCb simulation application, Gauss: Design, evolution and experience*, J. Phys. Conf. Ser. **331** (2011) 032023.
- [50] Particle Data Group, C. Patrignani *et al.*, *Review of particle physics*, Chin. Phys. **C40** (2016) 100001.
- [51] LHCb collaboration, R. Aaij *et al.*, *Prompt charm production in pp collisions at $\sqrt{s} = 7$ TeV*, Nucl. Phys. **B871** (2013) 1, [arXiv:1302.2864](#).
- [52] LHCb collaboration, R. Aaij *et al.*, *Measurements of prompt charm production cross-sections in pp collisions at $\sqrt{s} = 13$ TeV*, JHEP **03** (2016) 159, [arXiv:1510.01707](#).
- [53] T. Skwarnicki, *A study of the radiative cascade transitions between the Upsilon-prime and Upsilon resonances*, PhD thesis, Institute of Nuclear Physics, Krakow, 1986, DESY-F31-86-02.
- [54] LHCb collaboration, R. Aaij *et al.*, *Measurement of the track reconstruction efficiency at LHCb*, JINST **10** (2015) P02007, [arXiv:1408.1251](#).
- [55] J.-P. Lansberg and H.-S. Shao, *Towards an automated tool to evaluate the impact of the nuclear modification of the gluon density on quarkonium, D and B meson production in proton-nucleus collisions*, Eur. Phys. J. **C77** (2017) 1, [arXiv:1610.05382](#).
- [56] H.-S. Shao, *HELAC-Onia: An automatic matrix element generator for heavy quarkonium physics*, Comput. Phys. Commun. **184** (2013) 2562, [arXiv:1212.5293](#).

- [57] H.-S. Shao, *HELAC-Onia 2.0: an upgraded matrix-element and event generator for heavy quarkonium physics*, Comput. Phys. Commun. **198** (2016) 238, arXiv:1507.03435.
- [58] K. J. Eskola, H. Paukkunen, and C. A. Salgado, *EPS09: a new generation of NLO and LO nuclear parton distribution functions*, JHEP **04** (2009) 065, arXiv:0902.4154.
- [59] K. Kovarik *et al.*, *nCTEQ15 - Global analysis of nuclear parton distributions with uncertainties in the CTEQ framework*, Phys. Rev. **D93** (2016) 085037, arXiv:1509.00792.
- [60] H.-L. Lai *et al.*, *New parton distributions for collider physics*, Phys. Rev. **D82** (2010) 074024, arXiv:1007.2241.
- [61] LHCb collaboration, R. Aaij *et al.*, *Measurements of prompt charm production cross-sections in pp collisions at $\sqrt{s} = 5$ TeV*, arXiv:1610.02230, submitted to JHEP.
- [62] M. L. Mangano, P. Nason, and G. Ridolfi, *Heavy quark correlations in hadron collisions at next-to-leading order*, Nucl. Phys. **B373** (1992) 295.
- [63] D. Stump *et al.*, *Inclusive jet production, parton distributions, and the search for new physics*, JHEP **10** (2003) 046, arXiv:hep-ph/0303013.
- [64] B. Ducloué, T. Lappi, and H. Mäntysaari, *Forward J/ψ production in proton-nucleus collisions at high energy*, Phys. Rev. **D91** (2015) 114005, arXiv:1503.02789.
- [65] H. Fujii and K. Watanabe, *Nuclear modification of forward D production in pPb collisions at the LHC*, arXiv:1706.06728.
- [66] CMS collaboration, S. Chatrchyan *et al.*, *Observation of long-range near-side angular correlations in proton-lead collisions at the LHC*, Phys. Lett. **B718** (2013) 795, arXiv:1210.5482.
- [67] ALICE collaboration, B. Abelev *et al.*, *Long-range angular correlations on the near and away side in p-Pb collisions at $\sqrt{s_{NN}} = 5.02$ TeV*, Phys. Lett. **B719** (2013) 29, arXiv:1212.2001.
- [68] ATLAS collaboration, G. Aad *et al.*, *Observation of associated near-side and away-side long-range correlations in $\sqrt{s_{NN}} = 5.02$ TeV proton-lead collisions with the ATLAS detector*, Phys. Rev. Lett. **110** (2013) 182302, arXiv:1212.5198.
- [69] PHENIX collaboration, A. Adare *et al.*, *Quadrupole anisotropy in dihadron azimuthal correlations in central d+Au collisions at $\sqrt{s_{NN}}=200$ GeV*, Phys. Rev. Lett. **111** (2013) 212301, arXiv:1303.1794.
- [70] A. Beraudo *et al.*, *Heavy-flavour production in high-energy d-Au and p-Pb collisions*, JHEP **03** (2016) 123, arXiv:1512.05186.

LHCb collaboration

R. Aaij⁴⁰, B. Adeva³⁹, M. Adinolfi⁴⁸, Z. Ajaltouni⁵, S. Akar⁵⁹, J. Albrecht¹⁰, F. Alessio⁴⁰, M. Alexander⁵³, A. Alfonso Alberio³⁸, S. Ali⁴³, G. Alkhazov³¹, P. Alvarez Cartelle⁵⁵, A.A. Alves Jr⁵⁹, S. Amato², S. Amerio²³, Y. Amhis⁷, L. An³, L. Anderlini¹⁸, G. Andreassi⁴¹, M. Andreotti^{17,g}, J.E. Andrews⁶⁰, R.B. Appleby⁵⁶, F. Archilli⁴³, P. d'Argent¹², J. Arnau Romeu⁶, A. Artamonov³⁷, M. Artuso⁶¹, E. Aslanides⁶, G. Auriemma²⁶, M. Baalouch⁵, I. Babuschkin⁵⁶, S. Bachmann¹², J.J. Back⁵⁰, A. Badalov³⁸, C. Baesso⁶², S. Baker⁵⁵, V. Balagura^{7,c}, W. Baldini¹⁷, A. Baranov³⁵, R.J. Barlow⁵⁶, C. Barschel⁴⁰, S. Barsuk⁷, W. Barter⁵⁶, F. Baryshnikov³², M. Baszczyk^{27,l}, V. Batozskaya²⁹, V. Battista⁴¹, A. Bay⁴¹, L. Beaucourt⁴, J. Beddow⁵³, F. Bedeschi²⁴, I. Bediaga¹, A. Beiter⁶¹, L.J. Bel⁴³, N. Belyi⁶³, V. Bellee⁴¹, N. Belloli^{21,i}, K. Belous³⁷, I. Belyaev³², E. Ben-Haim⁸, G. Bencivenni¹⁹, S. Benson⁴³, S. Beranek⁹, A. Berezhnoy³³, R. Bernet⁴², D. Berninghoff¹², E. Bertholet⁸, A. Bertolin²³, C. Betancourt⁴², F. Betti¹⁵, M.-O. Bettler⁴⁰, M. van Beuzekom⁴³, I.a. Bezshyiko⁴², S. Bifani⁴⁷, P. Billoir⁸, A. Birnkraut¹⁰, A. Bitadze⁵⁶, A. Bizzeti^{18,u}, M.B. Bjoern⁵⁷, T. Blake⁵⁰, F. Blanc⁴¹, J. Blouw^{11,i}, S. Blusk⁶¹, V. Bocci²⁶, T. Boettcher⁵⁸, A. Bondar^{36,w}, N. Bondar³¹, W. Bonivento¹⁶, I. Bordyuzhin³², A. Borgheresi^{21,i}, S. Borghi⁵⁶, M. Borisyak³⁵, M. Borsato³⁹, M. Borysova⁴⁶, F. Bossu⁷, M. Boubdir⁹, T.J.V. Bowcock⁵⁴, E. Bowen⁴², C. Bozzi^{17,40}, S. Braun¹², T. Britton⁶¹, J. Brodzicka⁵⁶, D. Brundu¹⁶, E. Buchanan⁴⁸, C. Burr⁵⁶, A. Bursche^{16,f}, J. Buytaert⁴⁰, W. Byczynski⁴⁰, S. Cadeddu¹⁶, H. Cai⁶⁴, R. Calabrese^{17,g}, R. Calladine⁴⁷, M. Calvi^{21,i}, M. Calvo Gomez^{38,m}, A. Camboni³⁸, P. Campana¹⁹, D.H. Campora Perez⁴⁰, L. Capriotti⁵⁶, A. Carbone^{15,e}, G. Carboni^{25,j}, R. Cardinale^{20,h}, A. Cardini¹⁶, P. Carniti^{21,i}, L. Carson⁵², K. Carvalho Akiba², G. Casse⁵⁴, L. Cassina^{21,i}, L. Castillo Garcia⁴¹, M. Cattaneo⁴⁰, G. Cavallero^{20,40,h}, R. Cenci^{24,t}, D. Chamont⁷, M. Charles⁸, Ph. Charpentier⁴⁰, G. Chatzikonstantinidis⁴⁷, M. Chefdeville⁴, S. Chen⁵⁶, S.F. Cheung⁵⁷, S.-G. Chitic⁴⁰, V. Chobanova³⁹, M. Chrzaszcz^{42,27}, A. Chubykin³¹, X. Cid Vidal³⁹, G. Ciezarek⁴³, P.E.L. Clarke⁵², M. Clemencic⁴⁰, H.V. Cliff⁴⁹, J. Closier⁴⁰, V. Coco⁵⁹, J. Cogan⁶, E. Cogneras⁵, V. Cogoni^{16,f}, L. Cojocariu³⁰, P. Collins⁴⁰, T. Colombo⁴⁰, A. Comerma-Montells¹², A. Contu⁴⁰, A. Cook⁴⁸, G. Coombs⁴⁰, S. Coquereau³⁸, G. Corti⁴⁰, M. Corvo^{17,g}, C.M. Costa Sobral⁵⁰, B. Couturier⁴⁰, G.A. Cowan⁵², D.C. Craik⁵², A. Crocombe⁵⁰, M. Cruz Torres⁶², R. Currie⁵², C. D'Ambrosio⁴⁰, F. Da Cunha Marinho², E. Dall'Occo⁴³, J. Dalseno⁴⁸, A. Davis³, O. De Aguiar Francisco⁵⁴, K. De Bruyn⁶, S. De Capua⁵⁶, M. De Cian¹², J.M. De Miranda¹, L. De Paula², M. De Serio^{14,d}, P. De Simone¹⁹, C.T. Dean⁵³, D. Decamp⁴, L. Del Buono⁸, H.-P. Dembinski¹¹, M. Demmer¹⁰, A. Dendek²⁸, D. Derkach³⁵, O. Deschamps⁵, F. Dettori⁵⁴, B. Dey⁶⁵, A. Di Canto⁴⁰, P. Di Nezza¹⁹, H. Dijkstra⁴⁰, F. Dordei⁴⁰, M. Dorigo⁴¹, A. Dosil Suárez³⁹, L. Douglas⁵³, A. Dovbnya⁴⁵, K. Dreimanis⁵⁴, L. Dufour⁴³, G. Dujany⁸, K. Dungs⁴⁰, P. Durante⁴⁰, R. Dzhelyadin³⁷, M. Dziwiecki¹², A. Dziurda⁴⁰, A. Dzyuba³¹, N. Déléage⁴, S. Easo⁵¹, M. Ebert⁵², U. Egede⁵⁵, V. Egorychev³², S. Eidelman^{36,w}, S. Eisenhardt⁵², U. Eitschberger¹⁰, R. Ekelhof¹⁰, L. Eklund⁵³, S. Ely⁶¹, S. Esen¹², H.M. Evans⁴⁹, T. Evans⁵⁷, A. Falabella¹⁵, N. Farley⁴⁷, S. Farry⁵⁴, R. Fay⁵⁴, D. Fazzini^{21,i}, L. Federici²⁵, D. Ferguson⁵², G. Fernandez³⁸, P. Fernandez Declara⁴⁰, A. Fernandez Prieto³⁹, F. Ferrari¹⁵, F. Ferreira Rodrigues², M. Ferro-Luzzi⁴⁰, S. Filippov³⁴, R.A. Fini¹⁴, M. Fiore^{17,g}, M. Fiorini^{17,g}, M. Firlej²⁸, C. Fitzpatrick⁴¹, T. Fiutowski²⁸, F. Fleuret^{7,b}, K. Fohl⁴⁰, M. Fontana^{16,40}, F. Fontanelli^{20,h}, D.C. Forshaw⁶¹, R. Forty⁴⁰, V. Franco Lima⁵⁴, M. Frank⁴⁰, C. Frei⁴⁰, J. Fu^{22,q}, W. Funk⁴⁰, E. Furfaro^{25,j}, C. Färber⁴⁰, E. Gabriel⁵², A. Gallas Torreira³⁹, D. Galli^{15,e}, S. Gallorini²³, S. Gambetta⁵², M. Gandelman², P. Gandini⁵⁷, Y. Gao³, L.M. Garcia Martin⁷⁰, J. García Pardiñas³⁹, J. Garra Tico⁴⁹, L. Garrido³⁸, P.J. Garsed⁴⁹, D. Gascon³⁸, C. Gaspar⁴⁰, L. Gavardi¹⁰, G. Gazzoni⁵, D. Gerick¹², E. Gersabeck¹², M. Gersabeck⁵⁶, T. Gershon⁵⁰, Ph. Ghez⁴, S. Giani⁴¹, V. Gibson⁴⁹, O.G. Girard⁴¹, L. Giubega³⁰, K. Gizdov⁵², V.V. Gligorov⁸, D. Golubkov³², A. Golutvin^{55,40},

A. Gomes^{1,a}, I.V. Gorelov³³, C. Gotti^{21,i}, E. Govorkova⁴³, J.P. Grabowski¹², R. Graciani Diaz³⁸,
 L.A. Granado Cardoso⁴⁰, E. Graugés³⁸, E. Graverini⁴², G. Graziani¹⁸, A. Grecu³⁰, R. Greim⁹,
 P. Griffith¹⁶, L. Grillo^{21,40,i}, L. Gruber⁴⁰, B.R. Gruberg Cazon⁵⁷, O. Grünberg⁶⁷, E. Gushchin³⁴,
 Yu. Guz³⁷, T. Gys⁴⁰, C. Göbel⁶², T. Hadavizadeh⁵⁷, C. Hadjivasiliou⁵, G. Haefeli⁴¹, C. Haen⁴⁰,
 S.C. Haines⁴⁹, B. Hamilton⁶⁰, X. Han¹², T. Hancock⁵⁷, S. Hansmann-Menzemer¹², N. Harnew⁵⁷,
 S.T. Harnew⁴⁸, J. Harrison⁵⁶, C. Hasse⁴⁰, M. Hatch⁴⁰, J. He⁶³, M. Hecker⁵⁵, K. Heinicke¹⁰,
 A. Heister⁹, K. Hennessy⁵⁴, P. Henrard⁵, L. Henry⁷⁰, E. van Herwijnen⁴⁰, M. Heß⁶⁷,
 A. Hicheur², D. Hill⁵⁷, C. Hombach⁵⁶, P.H. Hopchev⁴¹, Z.-C. Huard⁵⁹, W. Hulsbergen⁴³,
 T. Humair⁵⁵, M. Hushchyn³⁵, D. Hutchcroft⁵⁴, P. Ibis¹⁰, M. Idzik²⁸, P. Ilten⁵⁸, R. Jacobsson⁴⁰,
 J. Jalocha⁵⁷, E. Jans⁴³, A. Jawahery⁶⁰, F. Jiang³, M. John⁵⁷, D. Johnson⁴⁰, C.R. Jones⁴⁹,
 C. Joram⁴⁰, B. Jost⁴⁰, N. Jurik⁵⁷, S. Kandybei⁴⁵, M. Karacson⁴⁰, J.M. Kariuki⁴⁸, S. Karodia⁵³,
 M. Kecke¹², M. Kelsey⁶¹, M. Kenzie⁴⁹, T. Ketel⁴⁴, E. Khairullin³⁵, B. Khanji¹²,
 C. Khurewathanakul⁴¹, T. Kirn⁹, S. Klaver⁵⁶, K. Klimaszewski²⁹, T. Klimovich¹¹, S. Koliiev⁴⁶,
 M. Kolpin¹², I. Komarov⁴¹, R. Kopecna¹², P. Koppenburg⁴³, A. Kosmyntseva³²,
 S. Kotriakhova³¹, M. Kozeiha⁵, L. Kravchuk³⁴, M. Kreps⁵⁰, P. Krokovny^{36,w}, F. Kruse¹⁰,
 W. Krzemien²⁹, W. Kucewicz^{27,l}, M. Kucharczyk²⁷, V. Kudryavtsev^{36,w}, A.K. Kuonen⁴¹,
 K. Kurek²⁹, T. Kvaratskheliya^{32,40}, D. Lacarrere⁴⁰, G. Lafferty⁵⁶, A. Lai¹⁶, G. Lanfranchi¹⁹,
 C. Langenbruch⁹, T. Latham⁵⁰, C. Lazzeroni⁴⁷, R. Le Gac⁶, J. van Leerdam⁴³, A. Leflat^{33,40},
 J. Lefrançois⁷, R. Lefèvre⁵, F. Lemaitre⁴⁰, E. Lemos Cid³⁹, O. Leroy⁶, T. Lesiak²⁷,
 B. Leverington¹², T. Li³, Y. Li⁷, Z. Li⁶¹, T. Likhomanenko^{35,68}, R. Lindner⁴⁰, F. Lionetto⁴²,
 X. Liu³, D. Loh⁵⁰, A. Loi¹⁶, I. Longstaff⁵³, J.H. Lopes², D. Lucchesi^{23,o}, M. Lucio Martinez³⁹,
 H. Luo⁵², A. Lupato²³, E. Luppi^{17,g}, O. Lupton⁴⁰, A. Lusiani²⁴, X. Lyu⁶³, F. Machefert⁷,
 F. Maciuc³⁰, V. Macko⁴¹, P. Mackowiak¹⁰, B. Maddock⁵⁹, S. Maddrell-Mander⁴⁸, O. Maev³¹,
 K. Maguire⁵⁶, D. Maisuzenko³¹, M.W. Majewski²⁸, S. Malde⁵⁷, A. Malinin⁶⁸, T. Maltsev³⁶,
 G. Manca^{16,f}, G. Mancinelli⁶, P. Manning⁶¹, D. Marangotto^{22,q}, J. Maratas^{5,v}, J.F. Marchand⁴,
 U. Marconi¹⁵, C. Marin Benito³⁸, M. Marinangeli⁴¹, P. Marino^{24,t}, J. Marks¹², G. Martellotti²⁶,
 M. Martin⁶, M. Martinelli⁴¹, D. Martinez Santos³⁹, F. Martinez Vidal⁷⁰, D. Martins Tostes²,
 L.M. Massacrier⁷, A. Massafferri¹, R. Matev⁴⁰, A. Mathad⁵⁰, Z. Mathe⁴⁰, C. Matteuzzi²¹,
 A. Mauri⁴², E. Maurice^{7,b}, B. Maurin⁴¹, A. Mazurov⁴⁷, M. McCann^{55,40}, A. McNab⁵⁶,
 R. McNulty¹³, J.V. Mead⁵⁴, B. Meadows⁵⁹, C. Meaux⁶, F. Meier¹⁰, N. Meinert⁶⁷,
 D. Melnychuk²⁹, M. Merk⁴³, A. Merli^{22,40,q}, E. Michielin²³, D.A. Milanese⁶⁶, E. Millard⁵⁰,
 M.-N. Minard⁴, L. Minzoni¹⁷, D.S. Mitzel¹², A. Mogini⁸, J. Molina Rodriguez¹,
 T. Mombacher¹⁰, I.A. Monroy⁶⁶, S. Monteil⁵, M. Morandin²³, M.J. Morello^{24,t}, O. Morgunova⁶⁸,
 J. Moron²⁸, A.B. Morris⁵², R. Mountain⁶¹, F. Muheim⁵², M. Mulder⁴³, M. Mussini¹⁵,
 D. Müller⁵⁶, J. Müller¹⁰, K. Müller⁴², V. Müller¹⁰, P. Naik⁴⁸, T. Nakada⁴¹, R. Nandakumar⁵¹,
 A. Nandi⁵⁷, I. Nasteva², M. Needham⁵², N. Neri^{22,40}, S. Neubert¹², N. Neufeld⁴⁰, M. Neuner¹²,
 T.D. Nguyen⁴¹, C. Nguyen-Mau^{41,n}, S. Nieswand⁹, R. Niet¹⁰, N. Nikitin³³, T. Nikodem¹²,
 A. Nogay⁶⁸, D.P. O’Hanlon⁵⁰, A. Oblakowska-Mucha²⁸, V. Obraztsov³⁷, S. Ogilvy¹⁹,
 R. Oldeman^{16,f}, C.J.G. Onderwater⁷¹, A. Ossowska²⁷, J.M. Otalora Goicochea², P. Owen⁴²,
 A. Oyanguren⁷⁰, P.R. Pais⁴¹, A. Palano^{14,d}, M. Palutan^{19,40}, A. Papanestis⁵¹, M. Pappagallo^{14,d},
 L.L. Pappalardo^{17,g}, C. Pappenheimer⁵⁹, W. Parker⁶⁰, C. Parkes⁵⁶, G. Passaleva¹⁸,
 A. Pastore^{14,d}, M. Patel⁵⁵, C. Patrignani^{15,e}, A. Pearce⁴⁰, A. Pellegrino⁴³, G. Penso²⁶,
 M. Pepe Altarelli⁴⁰, S. Perazzini⁴⁰, P. Perret⁵, L. Pescatore⁴¹, K. Petridis⁴⁸, A. Petrolini^{20,h},
 A. Petrov⁶⁸, M. Petruzzio^{22,q}, E. Picatoste Olloqui³⁸, B. Pietrzyk⁴, M. Pikiés²⁷, D. Pinci²⁶,
 A. Pistone^{20,h}, A. Piucci¹², V. Placinta³⁰, S. Playfer⁵², M. Plo Casasus³⁹, T. Poikela⁴⁰,
 F. Polci⁸, M. Poli Lener¹⁹, A. Poluektov^{50,36}, I. Polyakov⁶¹, E. Polcarpo², G.J. Pomery⁴⁸,
 S. Ponce⁴⁰, A. Popov³⁷, D. Popov^{11,40}, S. Poslavskii³⁷, C. Potterat², E. Price⁴⁸,
 J. Prisciandaro³⁹, C. Prouve⁴⁸, V. Pugatch⁴⁶, A. Puig Navarro⁴², H. Pullen⁵⁷, G. Punzi^{24,p},
 W. Qian⁵⁰, R. Quagliani^{7,48}, B. Quintana⁵, B. Rachwal²⁸, J.H. Rademacker⁴⁸, M. Rama²⁴,
 M. Ramos Pernas³⁹, M.S. Rangel², I. Raniuk^{45,†}, F. Ratnikov³⁵, G. Raven⁴⁴,

M. Ravonel Salzgeber⁴⁰, M. Reboud⁴, F. Redi⁵⁵, S. Reichert¹⁰, A.C. dos Reis¹,
C. Remon Alepuz⁷⁰, V. Renaudin⁷, S. Ricciardi⁵¹, S. Richards⁴⁸, M. Rihl⁴⁰, K. Rinnert⁵⁴,
V. Rives Molina³⁸, P. Robbe⁷, A.B. Rodrigues¹, E. Rodrigues⁵⁹, J.A. Rodriguez Lopez⁶⁶,
P. Rodriguez Perez^{56,†}, A. Rogozhnikov³⁵, S. Roiser⁴⁰, A. Rollings⁵⁷, V. Romanovskiy³⁷,
A. Romero Vidal³⁹, J.W. Ronayne¹³, M. Rotondo¹⁹, M.S. Rudolph⁶¹, T. Ruf⁴⁰, P. Ruiz Valls⁷⁰,
J. Ruiz Vidal⁷⁰, J.J. Saborido Silva³⁹, E. Sadykhov³², N. Sagidova³¹, B. Saitta^{16,f},
V. Salustino Guimaraes¹, D. Sanchez Gonzalo³⁸, C. Sanchez Mayordomo⁷⁰,
B. Sanmartin Sedes³⁹, R. Santacesaria²⁶, C. Santamarina Rios³⁹, M. Santimaria¹⁹,
E. Santovetti^{25,j}, G. Sarpis⁵⁶, A. Sarti²⁶, C. Satriano^{26,s}, A. Satta²⁵, D.M. Saunders⁴⁸,
D. Savrina^{32,33}, S. Schael⁹, M. Schellenberg¹⁰, M. Schiller⁵³, H. Schindler⁴⁰, M. Schlupp¹⁰,
M. Schmelling¹¹, T. Schmelzer¹⁰, B. Schmidt⁴⁰, O. Schneider⁴¹, A. Schopper⁴⁰, H.F. Schreiner⁵⁹,
K. Schubert¹⁰, M. Schubiger⁴¹, M.-H. Schune⁷, R. Schwemmer⁴⁰, B. Sciascia¹⁹, A. Sciubba^{26,k},
A. Semennikov³², A. Sergi⁴⁷, N. Serra⁴², J. Serrano⁶, L. Sestini²³, P. Seyfert⁴⁰, M. Shapkin³⁷,
I. Shapoval⁴⁵, Y. Shcheglov³¹, T. Shears⁵⁴, L. Shekhtman^{36,w}, V. Shevchenko⁶⁸, B.G. Siddi^{17,40},
R. Silva Coutinho⁴², L. Silva de Oliveira², G. Simi^{23,o}, S. Simone^{14,d}, M. Sirendi⁴⁹,
N. Skidmore⁴⁸, T. Skwarnicki⁶¹, E. Smith⁵⁵, I.T. Smith⁵², J. Smith⁴⁹, M. Smith⁵⁵,
I. Soares Lavra¹, M.D. Sokoloff⁵⁹, F.J.P. Soler⁵³, B. Souza De Paula², B. Spaan¹⁰, P. Spradlin⁵³,
S. Sridharan⁴⁰, F. Stagni⁴⁰, M. Stahl¹², S. Stahl⁴⁰, P. Stefko⁴¹, S. Stefkova⁵⁵, O. Steinkamp⁴²,
S. Stemmler¹², O. Stenyakin³⁷, H. Stevens¹⁰, S. Stone⁶¹, B. Storaci⁴², S. Stracka^{24,p},
M.E. Stramaglia⁴¹, M. Straticiu³⁰, U. Straumann⁴², L. Sun⁶⁴, W. Sutcliffe⁵⁵, K. Swientek²⁸,
V. Syropoulos⁴⁴, M. Szczekowski²⁹, T. Szumlak²⁸, M. Szymanski⁶³, S. T’Jampens⁴,
A. Tayduganov⁶, T. Tekampe¹⁰, G. Tellarini^{17,g}, F. Teubert⁴⁰, E. Thomas⁴⁰, J. van Tilburg⁴³,
M.J. Tilley⁵⁵, V. Tisserand⁴, M. Tobin⁴¹, S. Tolk⁴⁹, L. Tomassetti^{17,g}, D. Tonelli²⁴,
S. Topp-Joergensen⁵⁷, F. Toriello⁶¹, R. Tourinho Jadallah Aoude¹, E. Tournefier⁴, M. Traill⁵³,
M.T. Tran⁴¹, M. Tresch⁴², A. Trisovic⁴⁰, A. Tsaregorodtsev⁶, P. Tsopelas⁴³, A. Tully⁴⁹,
N. Tuning⁴³, A. Ukleja²⁹, A. Ustyuzhanin³⁵, U. Uwer¹², C. Vacca^{16,f}, A. Vagner⁶⁹,
V. Vagnoni^{15,40}, A. Valassi⁴⁰, S. Valat⁴⁰, G. Valenti¹⁵, R. Vazquez Gomez¹⁹,
P. Vazquez Regueiro³⁹, S. Vecchi¹⁷, M. van Veghel⁴³, J.J. Velthuis⁴⁸, M. Veltri^{18,r},
G. Veneziano⁵⁷, A. Venkateswaran⁶¹, T.A. Verlage⁹, M. Vernet⁵, M. Vesterinen⁵⁷,
J.V. Viana Barbosa⁴⁰, B. Viaud⁷, D. Vieira⁶³, M. Vieites Diaz³⁹, H. Viemann⁶⁷,
X. Vilasis-Cardona^{38,m}, M. Vitti⁴⁹, V. Volkov³³, A. Vollhardt⁴², B. Voneki⁴⁰, A. Vorobyev³¹,
V. Vorobyev^{36,w}, C. Vob⁹, J.A. de Vries⁴³, C. Vázquez Sierra³⁹, R. Waldi⁶⁷, C. Wallace⁵⁰,
R. Wallace¹³, J. Walsh²⁴, J. Wang⁶¹, D.R. Ward⁴⁹, H.M. Wark⁵⁴, N.K. Watson⁴⁷,
D. Websdale⁵⁵, A. Weiden⁴², M. Whitehead⁴⁰, J. Wicht⁵⁰, G. Wilkinson^{57,40}, M. Wilkinson⁶¹,
M. Williams⁵⁶, M.P. Williams⁴⁷, M. Williams⁵⁸, T. Williams⁴⁷, F.F. Wilson⁵¹, J. Wimberley⁶⁰,
M.A. Winn⁷, J. Wishahi¹⁰, W. Wislicki²⁹, M. Witek²⁷, G. Wormser⁷, S.A. Wotton⁴⁹,
K. Wraight⁵³, K. Wyllie⁴⁰, Y. Xie⁶⁵, Z. Xu⁴, Z. Yang³, Z. Yang⁶⁰, Y. Yao⁶¹, H. Yin⁶⁵, J. Yu⁶⁵,
X. Yuan⁶¹, O. Yushchenko³⁷, K.A. Zarebski⁴⁷, M. Zavertyaev^{11,c}, L. Zhang³, Y. Zhang⁷,
A. Zhelezov¹², Y. Zheng⁶³, X. Zhu³, V. Zhukov³³, J.B. Zonneveld⁵², S. Zucchelli¹⁵.

¹Centro Brasileiro de Pesquisas Físicas (CBPF), Rio de Janeiro, Brazil

²Universidade Federal do Rio de Janeiro (UFRJ), Rio de Janeiro, Brazil

³Center for High Energy Physics, Tsinghua University, Beijing, China

⁴LAPP, Université Savoie Mont-Blanc, CNRS/IN2P3, Annecy-Le-Vieux, France

⁵Clermont Université, Université Blaise Pascal, CNRS/IN2P3, LPC, Clermont-Ferrand, France

⁶CPPM, Aix-Marseille Université, CNRS/IN2P3, Marseille, France

⁷LAL, Université Paris-Sud, CNRS/IN2P3, Orsay, France

⁸LPNHE, Université Pierre et Marie Curie, Université Paris Diderot, CNRS/IN2P3, Paris, France

⁹I. Physikalisches Institut, RWTH Aachen University, Aachen, Germany

¹⁰Fakultät Physik, Technische Universität Dortmund, Dortmund, Germany

¹¹Max-Planck-Institut für Kernphysik (MPIK), Heidelberg, Germany

¹²Physikalisches Institut, Ruprecht-Karls-Universität Heidelberg, Heidelberg, Germany

- ¹³*School of Physics, University College Dublin, Dublin, Ireland*
- ¹⁴*Sezione INFN di Bari, Bari, Italy*
- ¹⁵*Sezione INFN di Bologna, Bologna, Italy*
- ¹⁶*Sezione INFN di Cagliari, Cagliari, Italy*
- ¹⁷*Universita e INFN, Ferrara, Ferrara, Italy*
- ¹⁸*Sezione INFN di Firenze, Firenze, Italy*
- ¹⁹*Laboratori Nazionali dell'INFN di Frascati, Frascati, Italy*
- ²⁰*Sezione INFN di Genova, Genova, Italy*
- ²¹*Universita e INFN, Milano-Bicocca, Milano, Italy*
- ²²*Sezione di Milano, Milano, Italy*
- ²³*Sezione INFN di Padova, Padova, Italy*
- ²⁴*Sezione INFN di Pisa, Pisa, Italy*
- ²⁵*Sezione INFN di Roma Tor Vergata, Roma, Italy*
- ²⁶*Sezione INFN di Roma La Sapienza, Roma, Italy*
- ²⁷*Henryk Niewodniczanski Institute of Nuclear Physics Polish Academy of Sciences, Kraków, Poland*
- ²⁸*AGH - University of Science and Technology, Faculty of Physics and Applied Computer Science, Kraków, Poland*
- ²⁹*National Center for Nuclear Research (NCBJ), Warsaw, Poland*
- ³⁰*Horia Hulubei National Institute of Physics and Nuclear Engineering, Bucharest-Magurele, Romania*
- ³¹*Petersburg Nuclear Physics Institute (PNPI), Gatchina, Russia*
- ³²*Institute of Theoretical and Experimental Physics (ITEP), Moscow, Russia*
- ³³*Institute of Nuclear Physics, Moscow State University (SINP MSU), Moscow, Russia*
- ³⁴*Institute for Nuclear Research of the Russian Academy of Sciences (INR RAN), Moscow, Russia*
- ³⁵*Yandex School of Data Analysis, Moscow, Russia*
- ³⁶*Budker Institute of Nuclear Physics (SB RAS), Novosibirsk, Russia*
- ³⁷*Institute for High Energy Physics (IHEP), Protvino, Russia*
- ³⁸*ICCUB, Universitat de Barcelona, Barcelona, Spain*
- ³⁹*Universidad de Santiago de Compostela, Santiago de Compostela, Spain*
- ⁴⁰*European Organization for Nuclear Research (CERN), Geneva, Switzerland*
- ⁴¹*Institute of Physics, Ecole Polytechnique Fédérale de Lausanne (EPFL), Lausanne, Switzerland*
- ⁴²*Physik-Institut, Universität Zürich, Zürich, Switzerland*
- ⁴³*Nikhef National Institute for Subatomic Physics, Amsterdam, The Netherlands*
- ⁴⁴*Nikhef National Institute for Subatomic Physics and VU University Amsterdam, Amsterdam, The Netherlands*
- ⁴⁵*NSC Kharkiv Institute of Physics and Technology (NSC KIPT), Kharkiv, Ukraine*
- ⁴⁶*Institute for Nuclear Research of the National Academy of Sciences (KINR), Kyiv, Ukraine*
- ⁴⁷*University of Birmingham, Birmingham, United Kingdom*
- ⁴⁸*H.H. Wills Physics Laboratory, University of Bristol, Bristol, United Kingdom*
- ⁴⁹*Cavendish Laboratory, University of Cambridge, Cambridge, United Kingdom*
- ⁵⁰*Department of Physics, University of Warwick, Coventry, United Kingdom*
- ⁵¹*STFC Rutherford Appleton Laboratory, Didcot, United Kingdom*
- ⁵²*School of Physics and Astronomy, University of Edinburgh, Edinburgh, United Kingdom*
- ⁵³*School of Physics and Astronomy, University of Glasgow, Glasgow, United Kingdom*
- ⁵⁴*Oliver Lodge Laboratory, University of Liverpool, Liverpool, United Kingdom*
- ⁵⁵*Imperial College London, London, United Kingdom*
- ⁵⁶*School of Physics and Astronomy, University of Manchester, Manchester, United Kingdom*
- ⁵⁷*Department of Physics, University of Oxford, Oxford, United Kingdom*
- ⁵⁸*Massachusetts Institute of Technology, Cambridge, MA, United States*
- ⁵⁹*University of Cincinnati, Cincinnati, OH, United States*
- ⁶⁰*University of Maryland, College Park, MD, United States*
- ⁶¹*Syracuse University, Syracuse, NY, United States*
- ⁶²*Pontifícia Universidade Católica do Rio de Janeiro (PUC-Rio), Rio de Janeiro, Brazil, associated to ²*
- ⁶³*University of Chinese Academy of Sciences, Beijing, China, associated to ³*
- ⁶⁴*School of Physics and Technology, Wuhan University, Wuhan, China, associated to ³*
- ⁶⁵*Institute of Particle Physics, Central China Normal University, Wuhan, Hubei, China, associated to ³*
- ⁶⁶*Departamento de Física, Universidad Nacional de Colombia, Bogota, Colombia, associated to ⁸*

- ⁶⁷ *Institut für Physik, Universität Rostock, Rostock, Germany, associated to* ¹²
⁶⁸ *National Research Centre Kurchatov Institute, Moscow, Russia, associated to* ³²
⁶⁹ *National Research Tomsk Polytechnic University, Tomsk, Russia, associated to* ³²
⁷⁰ *Instituto de Fisica Corpuscular, Centro Mixto Universidad de Valencia - CSIC, Valencia, Spain, associated to* ³⁸
⁷¹ *Van Swinderen Institute, University of Groningen, Groningen, The Netherlands, associated to* ⁴³

- ^a *Universidade Federal do Triângulo Mineiro (UFTM), Uberaba-MG, Brazil*
^b *Laboratoire Leprince-Ringuet, Palaiseau, France*
^c *P.N. Lebedev Physical Institute, Russian Academy of Science (LPI RAS), Moscow, Russia*
^d *Università di Bari, Bari, Italy*
^e *Università di Bologna, Bologna, Italy*
^f *Università di Cagliari, Cagliari, Italy*
^g *Università di Ferrara, Ferrara, Italy*
^h *Università di Genova, Genova, Italy*
ⁱ *Università di Milano Bicocca, Milano, Italy*
^j *Università di Roma Tor Vergata, Roma, Italy*
^k *Università di Roma La Sapienza, Roma, Italy*
^l *AGH - University of Science and Technology, Faculty of Computer Science, Electronics and Telecommunications, Kraków, Poland*
^m *LIFAELS, La Salle, Universitat Ramon Llull, Barcelona, Spain*
ⁿ *Hanoi University of Science, Hanoi, Viet Nam*
^o *Università di Padova, Padova, Italy*
^p *Università di Pisa, Pisa, Italy*
^q *Università degli Studi di Milano, Milano, Italy*
^r *Università di Urbino, Urbino, Italy*
^s *Università della Basilicata, Potenza, Italy*
^t *Scuola Normale Superiore, Pisa, Italy*
^u *Università di Modena e Reggio Emilia, Modena, Italy*
^v *Iligan Institute of Technology (IIT), Iligan, Philippines*
^w *Novosibirsk State University, Novosibirsk, Russia*
[†] *Deceased*